CHALMERS
UNIVERSITY OF TECHNOLOGY

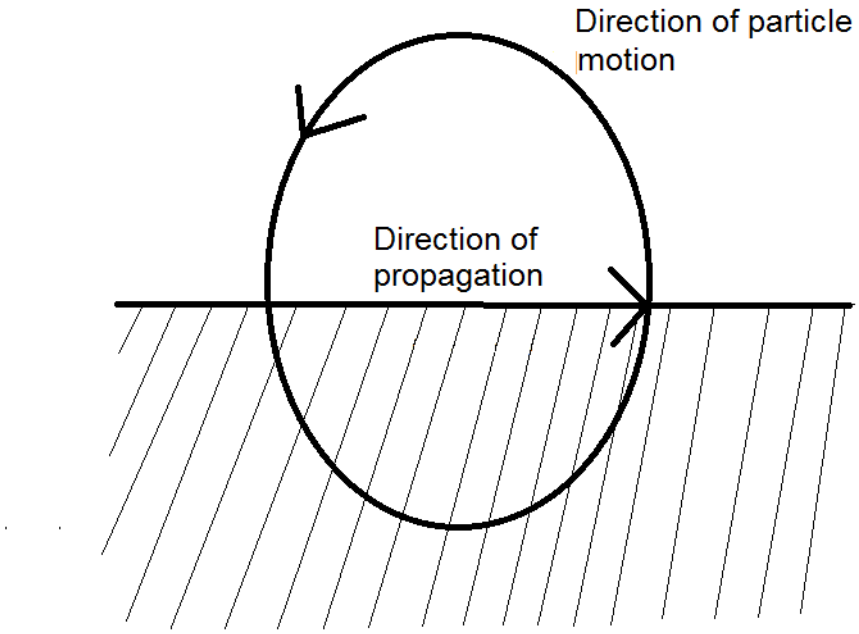

On the development of an SEA-model for a 3D-solid Theory and implementation

Master's Thesis in the Master's programme Sound and Vibration

Daniel Norgren

Department of Civil and Environmental Engineering
Division of Applied Acoustics
Vibroacoustics Group
CHALMERS UNIVERSITY OF TECHNOLOGY
Gothenburg, Sweden 2015
Master's Thesis 2015:6

MASTER'S THESIS 2015:6

On the development of an SEA-model for a 3D-solid

Theory and implementation

Master's Thesis in the Master's Programme Sound and Vibration

DANIEL NORGREN

Department of Civil and Environmental Engineering
Division of Applied Acoustics
Vibroacoustics Group
CHALMERS UNIVERSITY OF TECHNOLOGY

Göteborg, Sweden 2015

On the development of an SEA-model for a 3D-solid

Theory and implementation

Master's Thesis in the Master's Programme Sound and Vibration

DANIEL NORGREN

Examensarbete 2015:6/ Institutionen för bygg- och miljöteknik,
Chalmers Tekniska Högskola 2015

Department of Civil and Environmental Engineering
Division of Applied Acoustics
Vibroacoustics Group
Chalmers University of Technology
SE-412 96 Göteborg
Sweden
Telephone: +46 (0)31-772 1000

Cover:
Particle motion during propagation of a Rayleigh wave, see further information in sect. 2.7.
Department of Civil and Environmetal Engineering.Göteborg, Sweden, 2015

On the development of an SEA-model for a 3D-solid

Theory and implementation

Master's Thesis in the Master's Programme Sound and Vibration

DANIEL NORGREN Department of Civil and Environmental Engineering
Division of Applied Acoustics
Vibroacoustics Group
Chalmers University of Technology

ABSTRACT

The estimation of velocities and sound pressure levels, using the method of SEA - Statistical Energy Analysis, has been a long going technical issue. Previously, this technique has been used mostly in plates, having a 2D structure, and acoustic cavities, having a 3D structure. The goal of this report is to expand this theory for usage in modelling solid acoustic volumes such as e.g. a rock block or any other material. This further complicates the usage of SEA, introducing new boundary conditions, and the type of wave known as the Rayleigh wave. The model finally used in the SEA-analysis was chosen to be a cylinder of nylon (PA6GTECAST), because of the convenient size and properties of this object. When doing a study of the different waves present in a solid, having a bounding surface, it was found that the shear, longitudinal and Rayleigh waves were of importance. Of these, the longitudinal and Rayleigh waves were the ones actually implemented in the model. It was found that the distribution of energy between wave types, in a point excitation of a half-infinite solid, was of importance, due to the problem of determining which wave types are of interest to study. Another important factor was the transmission of the Rayleigh wave around a corner. The SEA-model was established using theory for predicting the distribution of energy between the waves present, and measuring and calculating SEA-parameters. This was not without problem, as the coupling loss factors needed to set up the model were based on previous research, not taking the coupling between Rayleigh waves and longitudinal or shear waves into account. This were suggested as a topic for future research. The results from measurements on the structure, with data for the 5 kHz band, were compared to the model results. It was stated that measuring the frequency response in a broader frequency interval, and comparing this to the model data, would be another topic for future research. This thesis is done in co-operation with Atlas Copco Rock Drills AB in Örebro.

Contents

Acknowledgements

I would like to thank Patrik Andersson, at Chalmers University of Technology, Division of Applied Acoustics, for his role as supervisor and examiner during this thesis. I would also like to thank Mattias Göthberg for his role as supervisor at Atlas Copco Rock Drills AB, and his great contributions to the theory, measurements and implementations performed during the work of this thesis. Furthermore, i would like to thank the whole division of Sound and Vibration at this company, for their support.

1 Introduction

In order to be able to model cases of drilling vibrations, which exists in today's mining business, companies such as Atlas Copco have a need for software to effectively do this. It is possible to use technique such as SEA - Statistical Energy Analysis. In figure 1, a drilling case in "Nackagruvan" below Nacka shopping center in Stockholm, is shown.

Figure 1: A drilling case in "Nackagruvan" below Nacka shopping center in Stockholm. [36]

The drilling process will affect the rock, leading to the formation of wave fronts, consisting of different types of waves. Of large importance is the Rayleigh wave, formed on the surface of the rock, or another media. The object finally chosen for the modelling process was a cylinder of nylon, due to the preferable vibrational properties of this object. This was basically because in SEA, you use the assumption that the wavelength is short in comparison with the dimensions of the structure, which will be the case for a nylon cylinder. This enabled modelling of a smaller, more convenient, object. In order to be able to make an SEA-model for this object, there were a few parameters that needed to be calculated or measured. This report focus on the properties of Rayleigh waves, and longitudinal waves, moving in the cylinder, and how these waves were implemented in the model. It also gives a brief look on some other types of waves that could potentially exist in an object similar to ours, i.e. shear waves, quasi-longitudinal waves and bending waves. Some literature were found to be important for the description of the different SEA-parameters and wave types, and these have been referred to throughout the report. The most

critical part, perhaps, of an SEA-analysis, is to model the coupling of the different wave types (sub-systems), which have been described in some detail in this report. Basically, this report aims at describing how it is possible to make an SEA-model for a 3D-type of structure, and compare it with measurements to validate it.

2 Theory

In this section, the basic wave types present in a half-infinite elastic media are presented. In addition, one find some information on wave types present in beams and plates. Also, the full derivation of the wave equation in 3D are described. Later, there is a deeper look-into the properties of Rayleigh waves travelling in different types of structures. It is also described how the energy of a point-excitation will distribute energy into different wave types. Statistical Energy Analysis, and it's parameters, are finally described in detail. These different theories are found in a number of different literature, that is referenced. It is notable that some of this literature cannot be used for more than study purposes, without having permission from the author. Most important, in source no. [26], it is clearly stated that the referenced material cannot be used for financial purposes, e. g. for making of a commercial SEA-software, without the author's permission.

2.1 Longitudinal waves moving in an elastic medium

The longitudinal wave moves in an elastic medium with the velocity [1]: $v_p = \sqrt{\frac{G(2-2\nu)}{\rho(1-2\nu)}}$

where G is the shear modulus of the media, ρ is the density of the media, and ν is Poisson's number of the media. The shear modulus is found from the formula:

$$G = \frac{E}{2(1+\nu)}$$

in which E is the young's modulus of the media.

The longitudinal wave affect the medium as a stretch or compression of the medium in the direction of propagation. Figure 2 shows the deformations caused in a medium, as a result of a longitudinal wave moving in one direction [3].

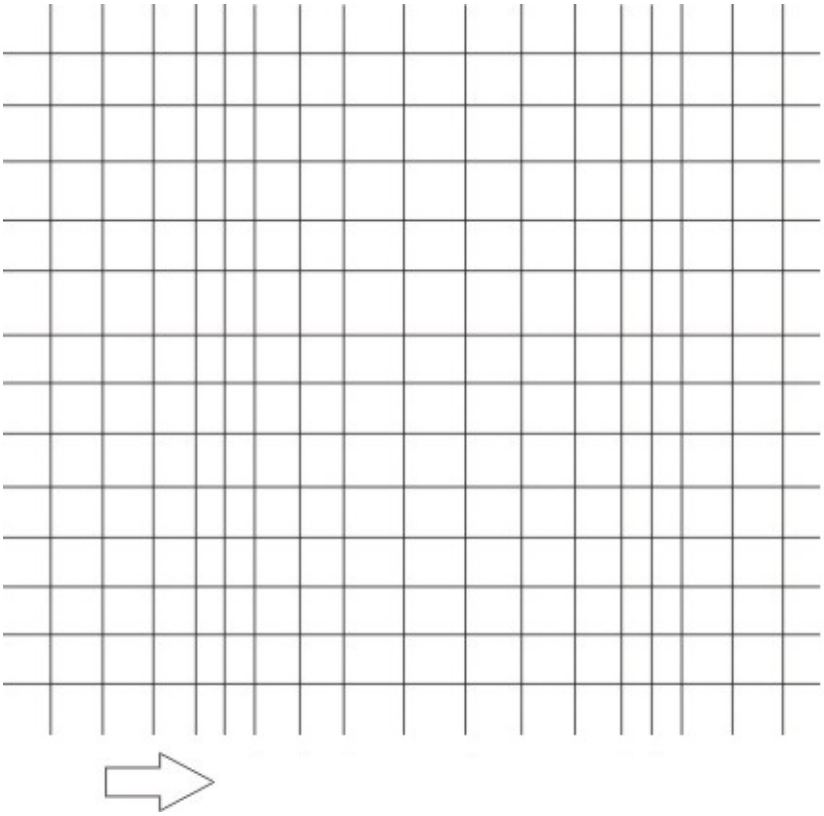

Figure 2: Longitudinal waves moving in a half-infinite elastic solid [3].

2.2 Shear waves moving in an elastic medium

A *transversal wave*, also known as a shear wave, moves through an elastic medium with velocity [1]:

$$v_t = \sqrt{\frac{G}{\rho}}$$

In opposite to the longitudinal wave, the shear wave does not change the volume of the element in which it moves [1]. The only thing that changes is the shape of the element, which undergoes a **shear deformation**. The shear waves travelling in the medium can move in any direction, not just paralell to the y or z-axis, which is also true for longitudinal waves. Combining these parts of displacement, the shear wave can move in an infinite number of directions.

If the velocities of the longitudinal waves and shear waves are compared, the following expression is obtained:

$$\frac{v_l}{v_t} = \sqrt{\frac{2-2v}{1-2v}}$$

In table 1, the wave velocities for longitudinal waves and shear waves, for a number of different medium, are given [3].

Material	Density (kg/m^3)	Longitudinal wave velocity (m/s)	Transverse wave velocity (m/s)
Metals			
Aluminium (rolled)	2700	6420	3040
Lead (rolled)	11400	2160	700
Gold	19700	3240	1200
Silver	10400	3640	1610
Copper (rolled)	8930	5010	2270
Copper (annealed)	8930	4760	2325
Magnesium	1740	5770	3050
Brass (70% Cu, 30% Zn)	8600	4700	2110
Steel (stainless)	7900	5790	3100
Steel (1% C)	7840	5940	3220
Zinc (rolled)	7100	4210	2440
Tin (rolled)	7300	3320	1670
Nonmetals			
Glass (Flint)	3600	4260	2552
Glass (Crown)	2500	5660	3391
Quartz, fused	2200	5968	3764
Plexiglas	1180	2680	1100
Polyethylene	900	1950	540
Polystyrene	1060	2350	1120

Table 1: The wave velocity for some common materials [3].

2.3 Bending waves moving in a beam

The phase velocity of bending waves moving in a beam is [16]:

$$c_b = \sqrt[4]{\frac{B}{\rho S}\omega^2} \quad (1)$$

in which $B = E \cdot I$ is the bending stiffness (I is the moment of inertia), and S is the area of the cross section.

The phase velocity increases as the root of the frequency increases [16]. The deviation in eq. (1) is approximately 10 % if the thickness of the beam is near to $\frac{1}{6}$ of the wavelength. Also, the group velocity for a bending wave is $c_{gb} = 2c_b$.

2.4 Quasi-longitudinal waves moving in a beam

Love wave, or quasi-longitudinal wave, is a type of surface wave present in beams. The motion of this wave is connected with the shear wave. The theory behind this wave type is described in detail in [21].

It is possible to study the wave equation to compute the bending of a thick and

infinite plate (or a beam where the width doesn't matter). First, the plate is studied. It is assumed, that waves only can move in the x-y-plane, as displayed in figure 3. Therefore, strain ϵ_z is put to zero.

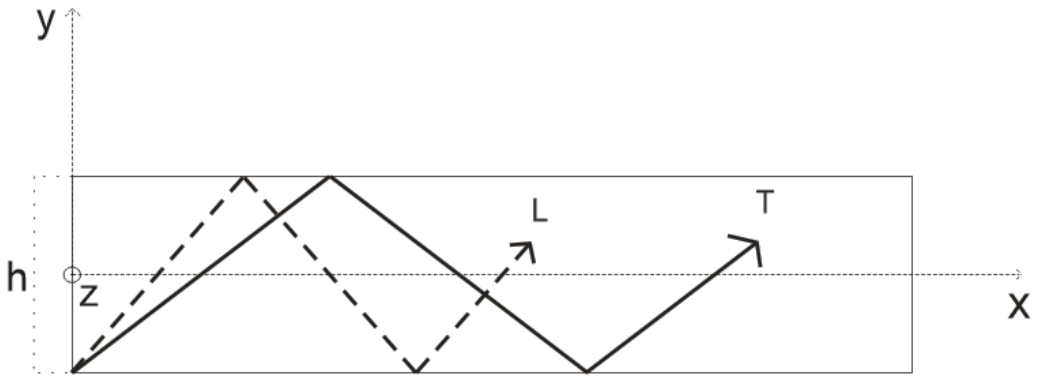

Figure 3: Love/transverse waves moving in the x-y-plane of a plate. [21]

The motion in the plate takes place as love- and transverse wave motion [21]. The surfaces of the plate, e.g. at $y = h/2$ or $y = -h/2$, will have a noticeable bending motion, due to the wave moving in the plate. The bending wave moving in the plate, can be described by:

$$A\exp\{i(\omega t - k_b x)\}$$

in which A is the amplitude, and k_b is the wave number of a bending wave. The wave number is dependent on the wavelength of the motion in the elastic medium, λ, by the equation:

$$k = \frac{2\pi}{\lambda}$$

The wave equation is governing the scalar potential ϕ, that models the love waves, and vector scalar potential Ξ, which describes the shear wave.

The scalar potential, which describes the love wave, is found to be:

$$\phi = \exp\{j(\omega t - k_b x)\}\{A_1 e^{-j\lambda_1 y} + A_2 e^{j\lambda_1 y}\} \quad (1)$$

in which A_1 is the amplitude of the wave moving towards the upper boundary, at $y = h/2$. A_2 is therefore the amplitude of the wave moving in direction of the lower boundary, at $y = -h/2$.

The potential ϕ is required to fulfill the wave equation for longitudinal waves. Therefore:

$$\lambda_1 = \sqrt{k_1^2 - k_b^2}$$

in which k_1 is the wave-number of a love wave, and:

$$k_1^2 = \frac{\omega^2\rho}{E}\frac{(1-\nu)(1-2\nu)}{(1-\nu)} = k_0^2\frac{(1-\nu)(1-\nu)}{(1-2\nu)}$$

It is found one vector potential that fulfills this condition, or more precisely it's

z-part, that describes the movement of the shear waves in the x-y-plane. It's in the form of:

$$\Xi_z = exp\{j\omega t - k_b x)\}\{A_3 e^{-j\lambda_2 y} + A_4 e^{j\lambda_2 y}\} \quad (2)$$

And this requires that the wave equation of the shear wave is fulfilled. Therefore:

$$\lambda_2 = \sqrt{k_t^2 - k_b^2}$$

$$k_t^2 = \frac{\omega^2 \rho 2(1+\nu)}{E} = k_0^2 \cdot 2(1-\nu)$$

It is possible to estimate, that for lower frequencies and thin plates, the wave number k_b is going to the wave number of a normal bending wave, κ_b. Therefore:

$$k_b \simeq \kappa_b > k_l$$

subsequently, the term λ_1 is complex in the lower frequencies. In order to simplify this discussion, the parameter α is described as:

$$\alpha = j\lambda_1 = \sqrt{k_b^2 - k_1^2}$$

The solution in (1) can therefore be rewritten as:

$$\phi_x = \exp\{i(\omega t - k_x x)\}\{B_1 \sinh(\alpha y + B_2 \cosh(\alpha y))\} \quad (3)$$

The vector potential in (2), has a z-part, that states the movement of the shear waves in the x-y-plane [21]. It is denoted as:

$$\psi_z = exp\{j(\omega t - k_x x)\}\{C_1 \sinh(\beta y) + C_2 \cosh(\beta y)\} \quad (4)$$

where:

$$\beta = \sqrt{k_b^2 - k_t^2}$$

The equation of ψ is qualified to fulfill the below wave equation, that is controlling the movement of these shear waves.

The displacements ζ and η, along the plus x- and y-axes , for $\psi_x = \psi_y = 0$, are found as:

$$\zeta = \frac{\partial \phi}{\partial x} + \frac{\partial \psi}{\partial y}$$

$$\eta = \frac{\partial \phi}{\partial y} - \frac{\partial \psi}{\partial x} \quad (5)$$

And the z part can be ignored.

Figure 4: a) in-phase motion of a plate (bending mode). b) anti-phase motion (longitudinal mode) [21].

There are two solutions to eq. (3) and (4). One denotes the in-phase motion and the other is the anti-phase motion of the boundaries of the plate. These different types of motion are described in figure 4. The in-phase motion corresponds to plate bending. For bending, there exists displacements normal to the boundary, where $y = \pm h/2$. These two parts are the same. But in x-direction, there is a contraction of one surface and lengthening of the other. Therefore, the in-phase motion, representing the mode of bending, can be described by:

$\zeta_+(y) = -\zeta_+(-y)$

$\eta_+(y) = \eta_+(-y)$ (6)

For the anti-phase motion, the following are found:

$\zeta_-(y) = \zeta_-(-y)$

$\eta_-(y) = -\eta_-(-y)$ (7)

Expression (6) says that the surfaces of the plate are moving in opposite direction, representing the displacement from a quasi-longitudinal wave. The subscripts that is described by + and - in (6) and (7) shows the motion in-phase, and anti-phase. This is seen in figure 4.

The quasi-longitudinal wave (for a thick plate, which is described on p.31 in [21]) has a wave number according to:

$k_b^2 = k_0^2(1-\nu^2) + \nu^2 h^2 k_0^4(1-\nu)/12 + ...$

The 1st two terms can be described by:

$k_b = k_1\sqrt{1 + \frac{\nu^2 h^2 k_1^2}{12(1-\nu^2)}}$

$k_1 = k_0\sqrt{1-\nu^2}$ (8)

This wave number is similar to the wave number of a bending wave, and it changes with the thickness of the plate, and frequency. The following condition is assumed to be fulfilled:

$h \to 0$, $k_x \to k_0 \cdot \sqrt{(1-\nu^2)}$

where k_x is the wave number for quasi-longitudinal waves moving in a thin plate. This means that the plate thickness are approaching zero, but still being a small value in comparison to the other dimensions of the plate. If the plate thickness, h is assumed to be larger, the 2nd and higher order terms must be taken into account. If the error in k_1 should be smaller than 10%, the wave number k_1 and the plate thickness h should fulfill:

$h\nu k_1(1-\nu) < 1.6$

If this condition is true, the plate can be seen as thin with respect to movement of longitudinal waves. The eq. (8) can be used to find the apparent density, ρ_a, of the plate as:

$$\rho_a = a \cdot [1 - \frac{\nu^2 h^2 k_1^2}{12(1-\nu^2)}] \quad (9)$$

Where a is the density of the plate. The app. density depends of the thickness of the plate and frequency. If the quota which is denoted as $\frac{\rho_a}{\rho}$, is bigger than 1, the displacement is also taking place normal to the main axis.

The 2D motion is increasing the inertia and therefore the mass, opposite to if only 1D motion is studied. And the wave number for a quasi-longitudinal wave can finally be expressed by:

$$k_1 = \omega\sqrt{\frac{\rho_a(1-\nu^2)}{E}} \quad (10)$$

2.5 Solution to the equation of motion for an elastic solid in 1D

The wave equation for an elastic solid in one dimension can be written as [1]: $\frac{\delta^2 u}{\delta t^2} = c^2 \frac{\delta^2 u}{\delta x^2}$

where u is denoted as the displacement of a wave moving in the medium, and c is the velocity of this wave.

This equation has solutions that come in the form of:

$u(x,t) = f(ct-x) + g(ct+x)$

These solutions can be used together with the wave number:

$k = \frac{\bar{\omega}}{c}$,

where $\bar{\omega}$ is the angular frequency of the loading on the body. This equation will then look as:

$u(x,t) = A\cos(\bar{\omega}t - kx) + B\cos(\bar{\omega}t + kx)$

Where A and B are complex constants given by the boundary conditions. If using

a complex form of notation the above equation can be simplified to:

$u(x,t) = Ce^{i(\bar{\omega}t-kx)} + De^{i(\bar{\omega}t+kx)}$

Where C and D are complex constants given by the boundary conditions.

2.6 Solution to the equation of motion for an elastic solid in 3D

In the case of waves traveling in a half-infinite solid, the three variables of concern are the elastic stresses, and the parts of displacements in 3D [1]. The parts of the displacements in respective x, y and z-direction, is ruled by three wave equations that are internally coupled to each other. The relevant variables for wave motion in a half-infinite elastic solid are thus:

- **Elastic shear stresses**, τ, and **elastic normal stresses**, σ
- **Parts of the displacements**, u, v, and w, in respective x, y, and z-direction

It is assumed, that longitudinal waves are travelling in the x-direction. This automatically makes the partial derivatives of the displacements in y and z-direction equal to zero. In opposite to this case, it is possible to assume that waves travelling in the medium are shear waves, with motion in the direction perpendicular to the direction of movement.

Three different wave types can exist in an half-infinite elastic solid, namely one longitudinal wave, and two shear waves (with the particle motion of each being perpendicular to the other one). The quota of the amplitudes of these waves is a function of the method of excitation. A solution for the wave equation described in the previons chapter can be extended to take into account a three dimensional elastic medium [1]. First, the shear stresses and normal stresses working on a piece of the medium, can be described.

Figure 5 shows a piece of a medium with lengths dx, dy and dz, with the normal stresses σ pointing outward from the cube, and the shear stresses τ pointing along the walls of the cube. The first letter after the respective stresses in figure 5 is denoted as the plane in which the stress is working, and the second letter denotes the direction in which it is working. The media shown in the figure is at rest and there is no external force doing work on the structure.

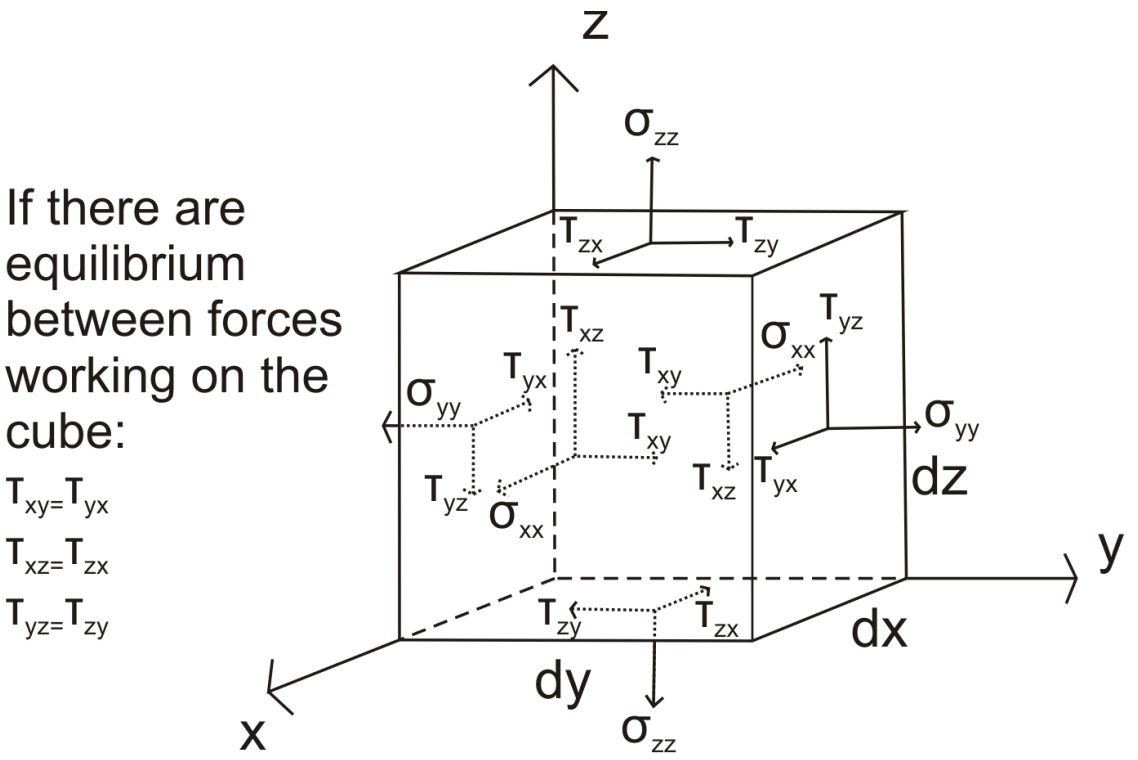

Figure 5: The normal and shear stresses working on a cube with sides dx, dy and dz.

In order to hold the balance of the forces working on the cube, it is possible to use the conditions shown in figure 5. These are:

$\tau xy = \tau yx$

$\tau xz = \tau zx$

$\tau yz = \tau zy$ (1)

These conditions can later be used, in order to obtain the governing equation of motion in each direction, x, y, and z. The description of stresses found in figure 5 can be extended to take into account the stress change in respective direction, due to a propagating wave. This is done by introducing partial derivatives, to be able to describe how the stresses affect the movement of the cube, when affected by a wave. Figure 6 shows the full analysis of the stresses working on the sides of the cube. In this figure, the letters u, v and w denotes the displacements in the x, y and z-direction, respectively.

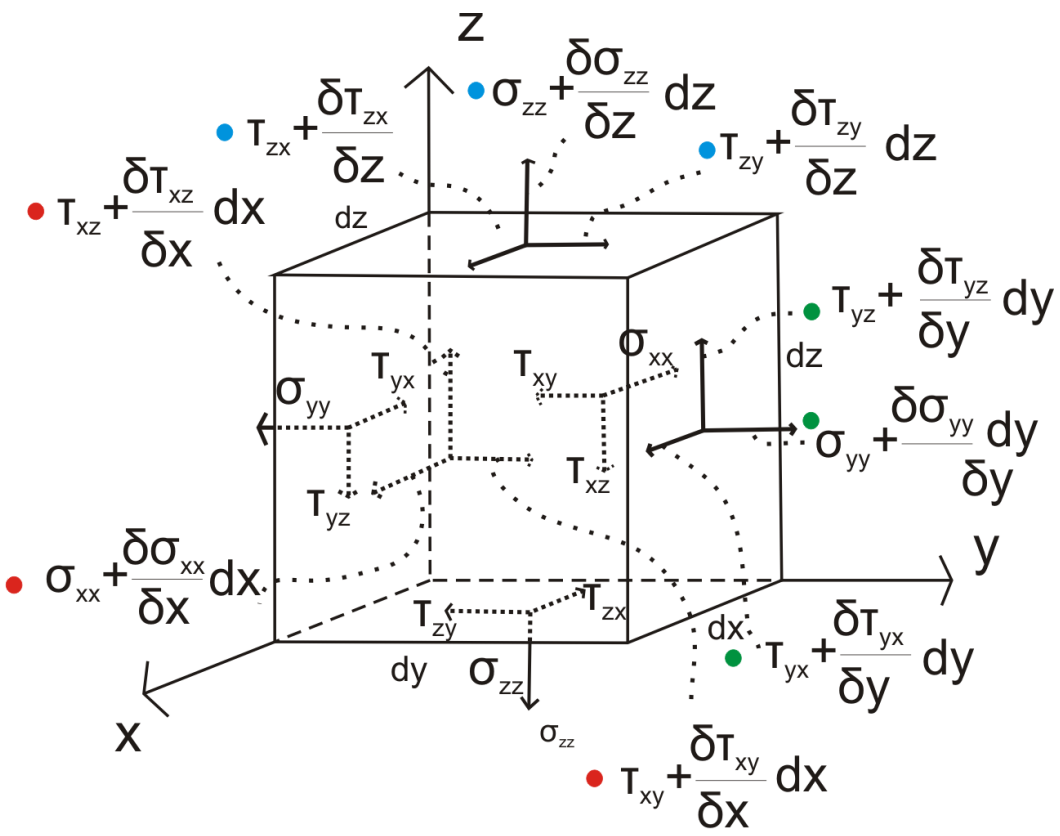

Figure 6: The full analysis of the normal and shear stresses working on a cube with sides dx, dy and dz.

First of all, a longitudinal wave travelling in x-direction, gives a change in the normal stress part at the distance dx from origo, and the total normal stress part at this face will be (marked with a red dot in figure 6):

$$\sigma_{xx} + \frac{\partial \sigma_{xx}}{\partial x} dx$$

Secondly, the shear stress parts working on the same face will have opposite direction, relative to the shear stress parts on the x-face, at origo, in order to hold the balance of the forces working on the cube. The change in stress at a distance dx from origo, as an effect of a shear wave travelling in x-direction, will result in the two total shear stress parts (marked with red dots in figure 6):

$$\tau_{xy} + \frac{\partial \tau_{xy}}{\partial x} dx,\ \tau_{xz} + \frac{\partial \tau_{xz}}{\partial x} dx$$

In the same manner, the normal stress part at a distance dz from origo will have a change, due to a longitudinal wave moving along the z-axis, resulting in a total part of (marked with a blue dot in figure 6):

$$\sigma_{zz} + \frac{\partial \sigma_{zz}}{\partial z} dz$$

The shear stress parts on this face will also be changed due to a shear wave moving in z-direction. The total parts will therefore be (marked with blue dots in the figure):

$\tau_{zx} + \frac{\partial \tau_{zx}}{\partial z} dz$, $\tau_{zy} + \frac{\partial \tau_{zy}}{\partial z} dz$

The normal stress part working on the face of the cube, on a distance dy from origo, will be changed, due to a longitudinal wave moving in y-direction (marked with green dots in figure 6):

$$\sigma_{yy} + \frac{\partial \sigma_{yy}}{\partial y} dy$$

The shear stress parts on this face will also experience a change due to a shear wave moving in y-direction. The total parts will therefore be (marked with green dots in the figure):

$\tau_{yx} + \frac{\partial \tau_{yx}}{\partial y} dy$, $\tau_{yz} + \frac{\partial \tau_{yz}}{\partial y} dy$

The total stresses working in the x-direction on the cube, as seen in figure 6, can be summed up according to:

$(\sigma_{xx} + \frac{\partial \sigma_{xx}}{\partial x} dx) dydz - \sigma_{xx} dydz + (\tau_{zx} + \frac{\partial \tau_{zx}}{\partial z} dz) dxdy - \tau_{zx} dxdy + (\tau_{yx} + \partial_{yx} + \frac{\partial \tau_{yx}}{\partial y} dydxdz - \tau_{yx} dxdz = \rho dxdydz \frac{\partial^2 u}{\partial t^2}$

Where the right hand term denotes the wave equation for an elastic solid in 3D, multiplied with the volume and density of the cube.

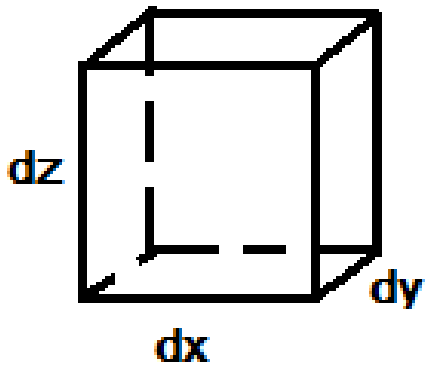

Figure 7: Infinitely small element of the cube.

By looking at an infinitely small element of the cube, as seen in figure 7, it is possible to remove all the non-zero elements dx, dy and dz from the formula. After this step, the following equation of motion is found [1]:

$$\frac{\partial \sigma_{xx}}{\partial x} + \frac{\partial \tau_{zx}}{\partial z} + \frac{\partial \tau_{yx}}{\partial y} = \rho \frac{\partial^2 u}{\partial t^2}$$

And if using the balance of the forces described in eq. (1), the following equation is found, which is the ruling equation of motion in x-direction:

$$\frac{\partial \sigma_{xx}}{\partial x} + \frac{\partial \tau_{xy}}{\partial z} + \frac{\partial \tau_{xz}}{\partial y} = \rho \frac{\partial^2 u}{\partial t^2}$$

Similar to this, it is possible to write the ruling equation of motion in the y-direction as:

$$\frac{\partial \tau_{yx}}{\partial x} + \frac{\partial \sigma_{yy}}{\partial z} + \frac{\partial \tau_{yz}}{\partial y} = \rho \frac{\partial^2 v}{\partial t^2}$$

and in z-direction, as:

$$\frac{\partial \tau_{zx}}{\partial x} + \frac{\partial \tau_{zy}}{\partial z} + \frac{\partial \sigma_{zz}}{\partial y} = \rho \frac{\partial^2 w}{\partial t^2}$$

2.7 Rayleigh waves on the surface of an elastic medium

As described earlier, if a medium reaches to infinity in all directions, basically two types of waves can move in it, and these are **longitudinal waves** and **shear waves**. If , however, the medium does not extend to infinity in one direction, but has a surface boundary, another type of wave is found, the **Rayleigh wave**. This is a kind of surface wave which moves on the surface of a half-infinite elastic medium. This wave consists of both longitudinal and transverse motion parts, which have a specific relation of the phases [2].

The amplitude of this type of motion declines rapidly in-depth of the medium. As the wave passes through the medium, the particles are moved in the form of an ellipse, and the largest axle of the ellipse lies in the plane that is vertical, as shown in figure 8. This is denoted as *retrograde* motion, and it is the opposite to the motion of a water wave, in which the particles move in the same direction as the wave propagates. The Rayleigh wave moves with a velocity that varies with the elastic parameters of the medium near the surface, but always fall below the shear wave velocity (for a plane surface).

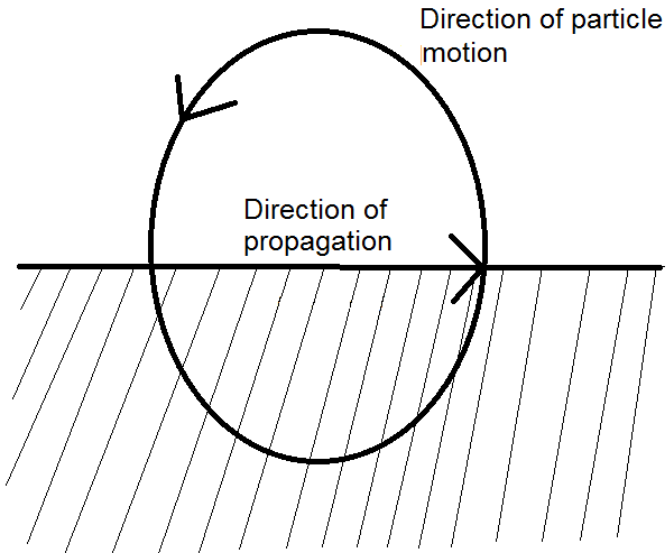

Figure 8: Particle motion during the movement of a Rayleigh wave.

In the case that the Rayleigh wave is harmonic, meaning that the wave form follows a specific sine-function during movement, with frequency ω and wave number k, it moves with a velocity:

$v = \frac{\omega}{k}$

in which k is the still unknown wave number of a Rayleigh wave.

It is of relevance to study the harmonic Rayleigh wave, moving in the boundary between an elastic, solid, isotropic and half-infinite media, and a vacuum [13]. The movement of the particles are shown in figure 9. The dots are the particles of the medium, and they are located at the same distance from each other, if there is no wave moving in the media. This medium is present in the region $z > 0$. If this area is filled with the half-infinite medium, a scalar potential ϕ, and vector potential ψ, can be used to model the Rayleigh wave. These are denoting the movement of the waves, giving the particles a displacement in vector notation:

$u = grad(\phi) + rot(\psi)$

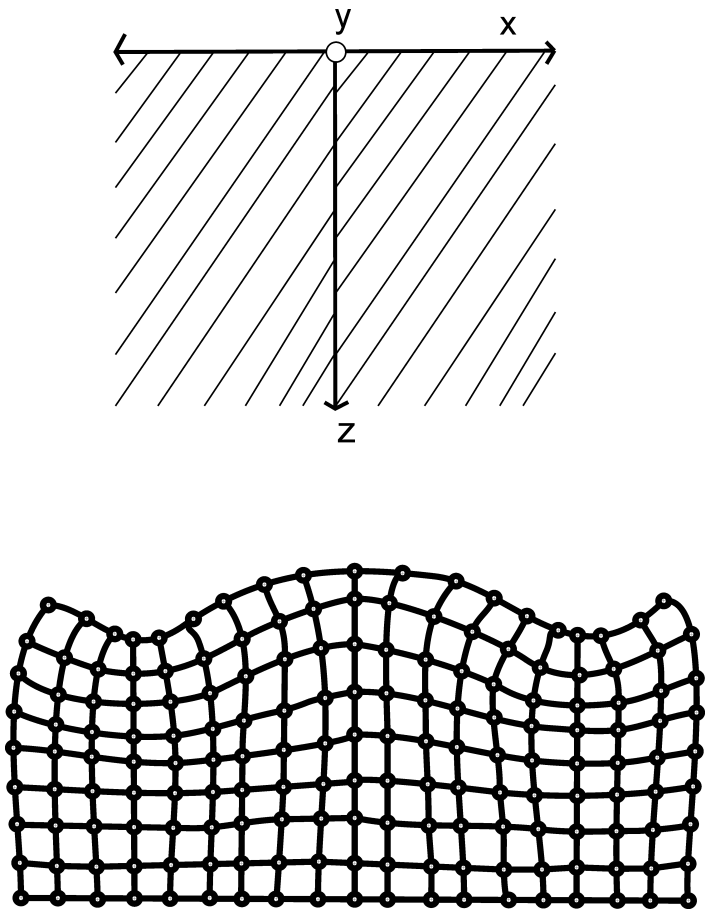

Figure 9: Particle movement while the Rayleigh wave is moving in the medium [13].

It is also possible to say that the wave is plane in regard to the y-axis, and in this

case, only the part of the vector potential along the y-axis will have values other than zero (ϕ). The potentials ϕ and ψ, can be seen as the potentials of longitudinal and shear waves, one by one. This is fulfilled in:

$$\frac{\partial^2\phi}{\partial x^2} + \frac{\partial^2\phi}{\partial z^2} + k_l^2\phi = 0 \ (1)$$

$$\frac{\partial^2\psi}{\partial x^2} + \frac{\partial^2\psi}{\partial z^2} + k_t^2\psi = 0 \ (2)$$

in which, $k_l = \omega\sqrt{\frac{\rho}{\lambda+2\mu}}$, $k_t = \omega\sqrt{\frac{\rho}{\mu}}$, are denoted the wave numbers of longitudinal- and shear waves, and λ and μ are Lame's coefficients. The particle displacement parts, along the x- and z-axis, are denoted as u and w. The parts of the stress, σ_{xx}, σ_{zz}, σ_{xz}, can be denoted in terms of ϕ, and ψ.

$$u = \frac{\partial\phi}{\partial x} - \frac{\partial\psi}{\partial z}$$

$$w = \frac{\partial\phi}{\partial z} - \frac{\partial\psi}{\partial x}$$

$$\sigma_{xx} = \lambda(\frac{\partial^2\phi}{\partial x^2} + \frac{\partial^2\phi}{\partial z^2}) + 2\mu(\frac{\partial^2\phi}{\partial x^2} - \frac{\partial^2\psi}{\partial x\partial z}) \ (3)$$

$$\sigma_{zz} = \lambda(\frac{\partial^2\phi}{\partial x^2} + \frac{\partial^2\phi}{\partial z^2}) + 2\mu(\frac{\partial^2\phi}{\partial z^2} + \frac{\partial^2\psi}{\partial x\partial z}) \ (4)$$

$$\sigma_{xz} = \nu_l(2\frac{\partial^2\phi}{\partial x\partial z} + \frac{\partial^2\psi}{\partial x^2} - \frac{\partial^2\phi}{\partial z^2}) \ (5)$$

It is of interest to solve equations (1) and (2), which denotes the harmonic longitudinal waves and shear waves, that are moving in the plus x-direction. This is found from:

$$\phi = F(z)e^{i(kx-\omega t)}$$

$$\psi = G(z)e^{i(kx-\omega t)}$$

If these formulas are put in (1) and (2), the following expressions are found:

$$\frac{d^2F(z)}{dz^2} - (k^2 - k_l^2)F(z) = 0$$

$$\frac{d^2G(z)}{dz^2} - (k^2 - k_t^2)G(z) = 0$$

And the terms that satisfy the equations above, are:

$$\exp(\pm\sqrt{k^2 - k_l^2})z = 0$$

$$\exp(\pm\sqrt{k^2 - k_t^2})z = 0$$

also, it is possible to assume that $k^2 < k_t^2 < k_l^2$. It is possible to look for a solution having plus roots in the exponent, and the result will give a movement which grows larger in-depth of the media. The other solution, having a minus root in the exponent, will give a movement growing smaller exponentially in-depth of the medium (e.g. a surface wave). The terms of ϕ, ψ, will be described as:

$\phi = Ae^{-qz}e^{i(kx-\omega t)}$

$\psi = Be^{-sz}e^{i(kx-\omega t)}$

in which $q^2 = k^2 - k_l^2$, $s^2 = k^2 - k_t^2$, and A, B are terms that can take on any values, but have a fixed relation to one another.

When describing the Rayleigh wave, the stresses σ_{zz}, σ_{xz}, should approach zero in the region of the boundary of the half-infinite medium (z=0, in figure 9). The connections between A, B, and k, which are the properties of the movement of the Rayleigh wave, are inserted into the formulas for ϕ and ψ, and this will give:

$\phi = -Ae^{i(kx-\omega t-qz)}$ (6)

$\psi = iA\frac{2kq}{k^2+s^2}e^{i(kx-\omega t-sz)}$ (7)

The relation formulating the wave number of a Rayleigh wave, k_r, has the form:

$4k^2qs - (k_r^2 + s^2) = 0$

And this relation is reduced to give:

$\eta^6 - 8\eta^4 + 8(3 - 2\xi^2)\eta^2 - 16(1 - \xi^2) = 0$ (8)

which has the notation: $\eta = \frac{k_t}{k_r} = \frac{c_r}{c_t}$, $\xi = \frac{k_l}{k_t} = \frac{c_t}{c_l}$. c_t, c_l are the phase velocities of longitudinal/shear waves. This relation is the **Rayleigh equation**. 6 roots can be found for this equation, which depends on the **Poisson's ratio**, ν, for the elastic medium. The root η_r, that lies between 0 and 1, is the root of the **Rayleigh wave**. For a ν in the common interval for real media ($0 < \nu < 0.5$), the eq. (8) has 1 root. Therefore, it is proven that a Rayleigh wave could be present on the surface of a half-infinite elastic medium. The root is estimated by:

$\eta_r = \frac{0.87+1.12\nu}{1+\nu}$

and the criteria $0 < \nu < 0.5$, says the phase velocity of the Rayleigh wave is between $0.87c_t$ and $0.96c_t$. Thus, it is proved that that the Rayleigh wave is **non-dispersive**, because η_r and c_t does not depend on frequency. The formulas (3) and (4), describing the stresses imposed by a Rayleigh wave, shows that it is made up of two non-homogeneous waves, longitudinal/shear, that moves along the boundary of the half-space with the same velocities. These two parts are damped in-depth according to:

$\exp(-\sqrt{k_r - k_l^2}z)$ (longitudinal part)

and: $\exp(-\sqrt{k_r - k_t^2}z)$ (shear part)

Close to the surface z=0 (the boundary of the half-infinite elastic medium), the stresses of the wave motion are going to zero. The following expressions describe the displacement parts in respective x and z-direction:

$$U_R = Ak_r(e^{(-q_r^z - \frac{2q_r s_r}{k_r^2+s_r^2}e^{-s_r^z})\sin(k_r x - \omega t)})$$

$$W_R = Aq_r(e^{(-q_r^z - \frac{2k_r^2}{k_r^2+s_r^2}e^{-s_r^z})\cos(k_r x - \omega t)})$$

The stress parts of the Rayleigh wave are found from (3), (4), (5), (6), (7).

In figure 10, the amplitudes of displacement, $\hat{U_R}$, $\hat{W_R}$, and the values of the stress, $\sigma\hat{z}z$, $\sigma\hat{x}x$, $\sigma\hat{x}z$, is related to depth of the media.

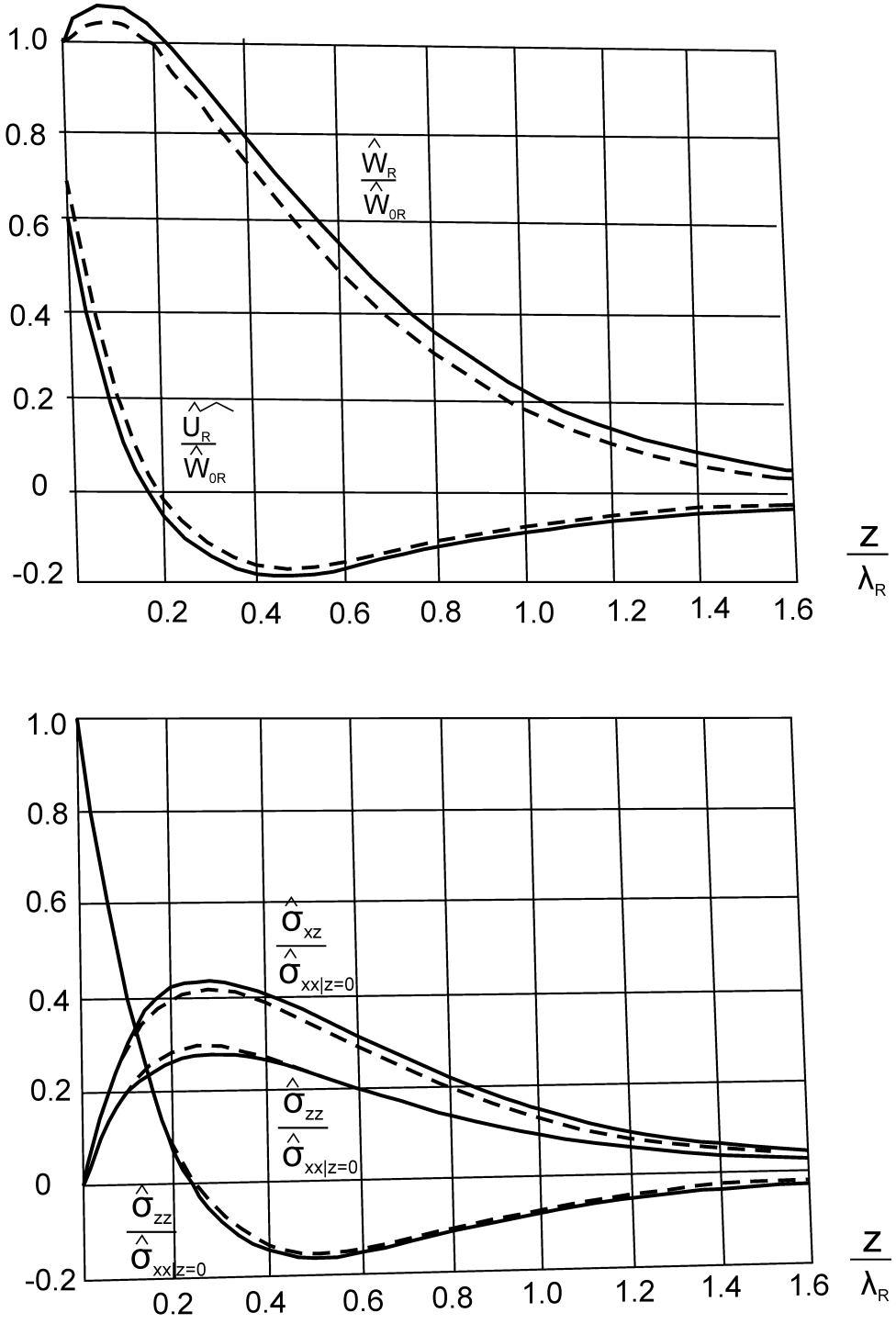

Figure 10: Amplitudes of displacement, $\hat{U_R}$, $\hat{W_R}$, and the values of the stress, $\sigma\hat{zz}$, $\sigma\hat{xx}$, $\sigma\hat{xz}$, related to depth of the media. [13]

The data in figure 10 have no dimension, and the values of the amplitudes are correlated to the displacement amplitude, $\hat{W}_{0R}$, on the surface, and the stress amplitudes $\hat{\sigma}_{xx|z=0}$, on the surface. The depth of the media is related to the wavelength. The data in figure 10 are given for two values of Poisson's number, $\nu = 0.25$ (dashes),

$\nu = 0.34$ (dots). Commonly, metals have a value of Poisson's ratio in this interval. It is seen in the graphs, that the displacement normal to the boundary increases first, than drops of over the depth, and the displacement parallel to the surface undergo a change of sign at a depth of close to $0.2\lambda_R$. Also, the term σ_{xx} undergo a change of sign, and σ_{zz}, σ_{xz} has maximum at around $\frac{z}{\lambda_R} = 0.3$, then decreases with the exponent over depth in the medium.

There is a phase difference of the displacement parts (x-axis/z-axis) of $\frac{\pi}{2}$. This means that the movement in the Rayleigh waves will be elliptic, as described earlier. The motion on the plus side of the x-axis (in figure 9), will give an elliptic circulation that moves equal to a clock, and the displacement will change sign at a depth of $z > 0.2\lambda_R$. This means that the particle movement of the Rayleigh wave will go in the opposite direction relative to the movement near the surface. The half-major axis of this motion are normal to the plane z=0, and the half-minor axis of this motion are parallel to this plane. The elliptic movement has an **eccentricity** that is varying with depth into the medium, and the Poisson's ratio of it. In table 2, the length of these half-axes are given in relation to the wavelength of a Rayleigh wave, for some numbers of ν. The upper part of the quota gives the size of the half-major axis, having amplitude $\hat{W_R}$, and the lower part of the quota gives the size of the half-minor axis, having amplitude $\hat{U_R}$.

$\frac{z}{\lambda_R}$	$\nu = 0$	$\nu = 0.250$	$\nu = 0.333$	$\nu = 0.500$
0	$\frac{1.000}{0.772}$	$\frac{1.000}{0.676}$	$\frac{1.000}{0.626}$	$\frac{1.000}{0.540}$
0.250	$\frac{0.745}{-0.007}$	$\frac{0.910}{-0.076}$	$\frac{0.968}{-0.101}$	$\frac{1.120}{-0.158}$
0.500	$\frac{0.432}{-0.104}$	$\frac{0.587}{-0.157}$	$\frac{0.643}{-0.177}$	$\frac{0.812}{-0.206}$
1.000	$\frac{0.109}{-0.044}$	$\frac{0.192}{-0.071}$	$\frac{0.219}{-0.077}$	$\frac{0.339}{-0.099}$

Table 2: The length of the half-axes in relation to the Rayleigh wave-length for some values of ν [13].

The most fundamental case of a harmonic and plane Rayleigh wave moving in a half-infinite elastic medium, has been described above. If, however, the medium is non-homogeneous and have different properties in different directions, the Rayleigh waves differ from the simpler case. In case of some of these non-isotropic mediums, e.g. triclinic crystals, there are in most cases no Rayleigh waves present. Between a solid and a fluid, e.g. rock/air, there always exists Rayleigh waves. In other cases they are only found for certain relations between the elastic and geometric properties of the mediums.

In figure 11, the Rayleigh wave velocity over Poisson's number is given [3].

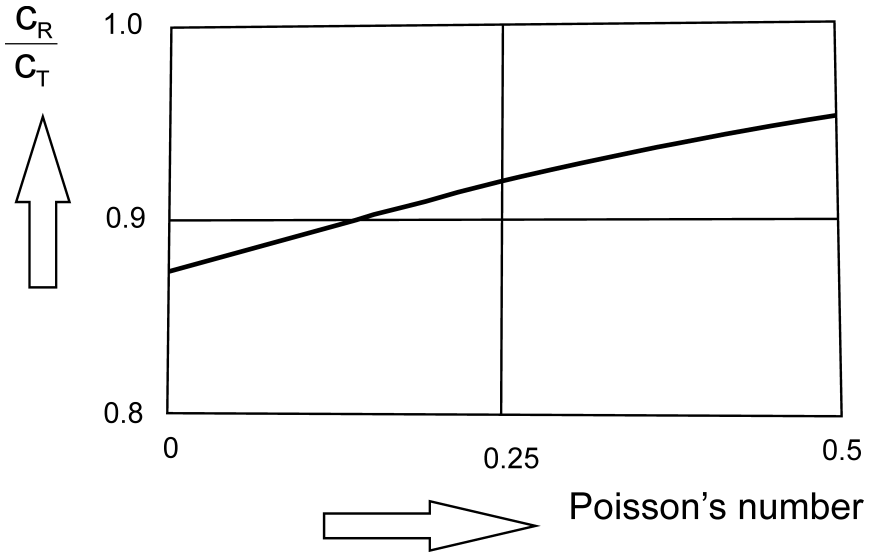

Figure 11: The Rayleigh wave velocity over Poisson's number [3].

and the different types of waves can then be related to each other with respect to Poisson's number of the medium, using the shear wave velocity as a reference value. This is shown in figure 12 [1].

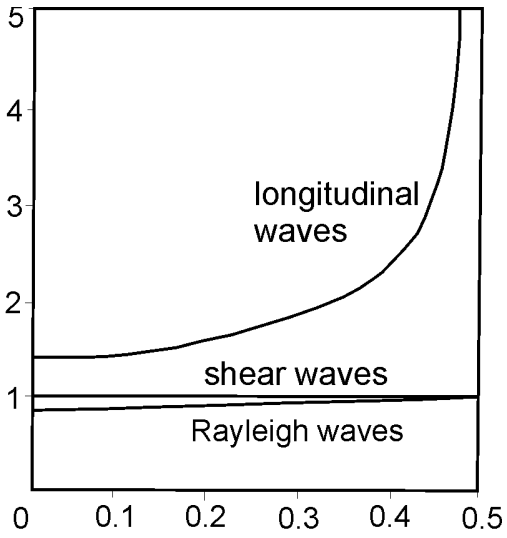

Figure 12: Relation between the different wave velocities as a fuction of Poisson's number of the medium. [1]

The Rayleigh wave can originate in a number of different sources, as localized strikes or point-force excitation. In earthquakes, these kind of waves are created on the surface of the earth. If these waves are moving in a layer, they are referred to as **Lamb waves**.

2.7.1 Effect of the curving radius on the Rayleigh wave

The method for calculating the velocity of a Rayleigh wave on a surface that is curved, is derived in [23]. This calculation is quite long, so it will not be given in detail here. It is a deepening recommended for those with strong skills in technical physics. The following part is basically the summary part of paper [23].

It is possible to use the relation between wave velocity, wave number and frequency: $k_l = \frac{\omega}{c_l}$, $k_t = \frac{\omega}{c_t}$, and $k_0 = \frac{\omega}{c_r}$, where c_l, c_t are denoted as the longitudinal and shear wave velocity of the volume waves, and c_r is denoted as the phase velocity of a surface wave on a flat partition.

It is stated that ρ is the density of the material, and $c_l^2 = (\lambda+2\mu)/\rho$, $c_t^2 = \frac{\mu}{\rho}$, where μ and λ are Lame's constants. The following formula is a correctional term for the radius of curving [23]:

$$\delta = \frac{1}{k_0 C'}\left(\frac{A'}{\rho_\alpha} + \frac{B'}{\rho_\beta}\right). \quad (23)$$

in which:

$$A' = 2c_1^2\sqrt{1 - \frac{c_r^2}{c_1^2}} - c_r^2\sqrt{1 - \frac{c_r^2}{c_t^2}},$$

$$B' = -2c_t^2\left(\frac{c_r^2}{c_1^2 - c_r^2}\sqrt{1 - \frac{c_r^2}{c_t^2}} + \frac{c_t^2}{c_t^2 - c_r^2}\sqrt{1 - \frac{c_r^2}{c_l^2}}\right),$$

$$C' = 2(3c_r^2 - 5c_t^2).$$

and ρ_α and ρ_β are the radius of curving in α and β-direction, respectively. This is explained by looking at figure 13.

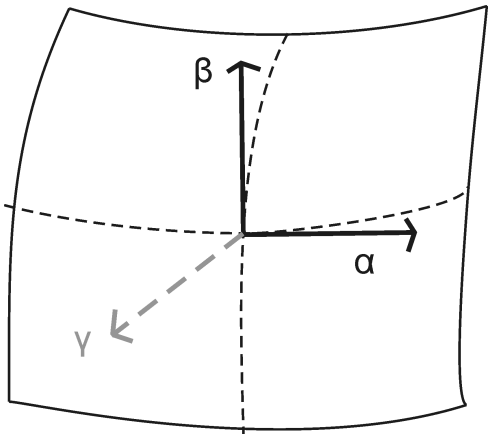

Figure 13: The cartesian coordinates used on the curved surface. [23]

It is possible to denote this correction term as δ_C. The velocity of a Rayleigh wave on a curved surface is denoted c, and it is related to the velocity of a Rayleigh wave on a flat surface, c_r, according to:

$c = c_r(1 - \delta_c)$.

The velocity of a Rayleigh wave on a curved surface can also be expressed as $c = \omega/k$, where the wave number of the Rayleigh wave, k, on a curved surface, is:

$k = k_0(1 + \delta)^{1/2}$

Thus, the velocity of a Rayleigh wave on a curved surface can be expressed as:

$c = \frac{\omega}{k_0(1+\delta)^{1/2}} \approx \frac{\omega}{k_0}(1 - \frac{1}{2}\delta) = c_r(1 - \frac{1}{2}\delta)$

and subsequently:

$\delta_c = -\frac{1}{2}\delta = -\frac{1}{2}\frac{1}{k_0 C'}(\frac{A'}{\rho_\alpha} + \frac{B'}{\rho_\beta})$. (24)

And this formula relates the surface wave phase velocity, and curving, $\frac{1}{\rho_\alpha}$, $\frac{1}{\rho_\beta}$.

2.7.2 Transmission coefficient for Rayleigh waves over a wedge

In literature [26], the case of Rayleigh wave transmission of a 90^o wedge is studied. In the search for literature, other sources for similar derivations were found, among them [27], and [28], but the method described in this section was found to be the most suitable.

The quarter space in figure 14 is considered.

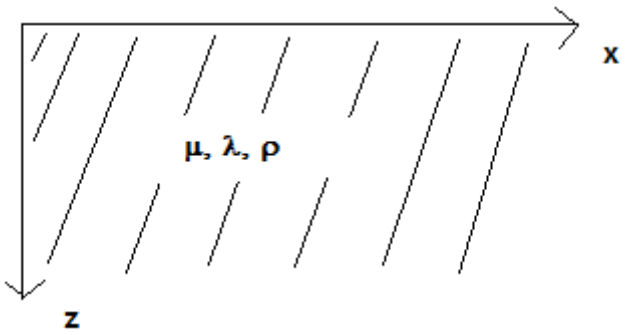

Figure 14: The quarter space problem. [26]

It can be assumed that a Rayleigh wave is moving towards the corner, in minus x-direction, incoming at the boundary of the two planes, $x = 0$. The longitudinal wave velocity is denoted by α, the shear wave velocity by β, and the Rayleigh wave velocity by γ. The Rayleigh wave, which is incoming towards the corner, in minus x-direction, and the Rayleigh wave which is reflected at this corner, can be described by the potentials:

$\phi = A_1 e^{-rz} e^{j(\omega t + k_\gamma x)} + A_2 e^{-rz} e^{j(\omega t - k_\gamma x)}$

$\psi = B_1 e^{-sz} e^{j(\omega t + k_\gamma x)} + B_2 e^{-sz} e^{j(\omega t - k_\gamma x)}$ (1)

where A_1 and B_1 are the amplitudes of the incoming wave, and A_2 and B_2 are the

amplitudes of the reflected wave.

In the above expression,

$r^2 = k_\gamma^2 - k_\alpha^2$, $s^2 = k_\gamma^2 - k_\beta^2$

The amplitude B_1 is determined by A_1, and the amplitude $B_2$is determined by A_2, which means that there are only 2 unknowns in (1). When looking at the boundary conditions, the stresses in both normal and tangential direction, p_{xx} and p_{xz}, should be zero on the boundary of the two planes, $x = 0$. But no selection of A_2, or B_2, will fulfill these terms. Because of this, the following method of working is suggested:

It is possible to perform an estimation of the amplitude of the reflected Rayleigh wave, at the boundary of both planes. It can be done by selecting this amplitude from the condition that the stress at the surface of reflection ($x = 0$), are minimized by the method of least squares. But the volume waves created by this reflection are omitted. Therefore, the reflection coefficient $R = A_2/A_1$ are selected to fulfill:

$\int_0^\infty = |p_{xx}|^2 + |p_{xz}|^2 dz$ (2)

with a minimum at x=0.

These are the formulations of the stress and displacement equations for a medium of isotropic properties:

$p_{xx} = \lambda\theta + 2\mu\frac{du}{dx}; p_{xy} = \mu(\frac{du}{dy} + \frac{dv}{dx})$

$p_{yy} = \lambda\theta + 2\mu\frac{dv}{dy}; p_{yz} = \mu(\frac{dv}{dz} + \frac{dw}{dy})$

$p_{zz} = \lambda\theta + 2\mu\frac{dw}{dz}; p_{zx} = \mu(\frac{dw}{dx} + \frac{du}{dz})$ (3)

in which $\theta = \nabla \cdot \overrightarrow{D}$, and $\overrightarrow{D}$ is the displacement parts in x- y- and z-direction, described by the scalar potential ϕ and vector potential $\overrightarrow{\psi}(\psi_1, \psi_2, \psi_3)$, according to:

$u = \frac{\partial\phi}{\partial x} + \frac{\partial\psi_3}{\partial y} - \frac{\partial\psi_2}{\partial z}$

$v = \frac{\partial\phi}{\partial y} + \frac{\partial\psi_1}{\partial z} - \frac{\partial\psi_3}{\partial x}$

$w = \frac{\partial\phi}{\partial z} + \frac{\partial\psi_2}{\partial x} - \frac{\partial\psi_1}{\partial y}$

or in notation of vectors:

$\overrightarrow{D}(u, v, w) = \nabla\phi + \nabla\cdot\overrightarrow{\psi}(\psi_1, \psi_2, \psi_3)$

The expressions for the two stresses, which are relevant for the Rayleigh wave, can be found by looking at formula (1), together with formula (3):

$p_{xx} = -\mu(2r^2 + k_\beta^2)(A_1 + A_2)e^{-rz} + 2\mu jk_\gamma s(B_1 - B_2)e^{-sz}$

$$p_{xz} = 2\mu j k_\gamma r(A_1 + A_2)e^{-rz} - \mu(2s^2 + k_\beta^2(B_1 + B_2)e^{-sz} \quad (4)$$

It is possible to use the relationship between A and B, which is determined from the conditions at the boundary. This relation is found by assuming that the planes bounding the quarter-space lies next to a media free of stresses (e.g air). Therefore, the stresses p_{zy}, p_{zz}, and p_{xz} must be zero at z=0. This means that there will be no motion in the y-direction. And the following expressions are found for the arbitrary constants A and B:

$$(2k_\gamma^2 - k_\beta^2)A + 2jk_\gamma sB = 0$$

$$-2jk_\gamma rA + (2k_\gamma^2 - k_\beta^2)B = 0 \quad (5)$$

It is desirable to find values of A, B $\neq 0$, and this requires that the Rayleigh equation is satisfied (see section 2.7).

Incorporating the relationship between A and B, that is found in (5), the equation (4) will be reduced to:

$$p_{xx}/A = -\mu(1 - R)(ae^{-rz} - be^{-sz})$$

$$p_{xz}/A = -2\mu j k_\gamma r(1 - R)(e^{-rz} - e^{-sz}) \quad (6)$$

in which it is possible to denote a and b, by:

$$a = 2r^2 + k_\beta^2;\ b = 2s^2 + k_\beta^2$$

Then it is possible to look at integral (2), of which we want to find a minima. This can be described, using the introduced notation, by:

$$I = \frac{1}{A_1^2}\int_0^\infty |p_{xx}|^2 + |p_{xz}|^2 dz = \mu^2(1-R)^2(\frac{a^2}{2r} - \frac{2ab}{r+s} + \frac{b^2}{2s}) + 4\mu^2 k_\gamma^2 r^2(1-R)^2(\frac{1}{2r} - \frac{2}{r+s} + \frac{1}{2s}) = M(1 - R)^2 + N(1 - R)^2$$

in which M and N have a dependence of the frequency, Young's modulus, Poisson's ratio and density of the material.

The next step is to look at the minima, $\frac{dI}{dR} = 0$, and find a solution to this equation with respect to R. This will give:

$$R = \frac{N-M}{N+M}$$

There is no dependence of R upon the frequency, ω, because this will disappear by the ratio $\frac{N-M}{N+M}$. It makes sense, because there is no length defining the geometry of this problem.

In order to find the factor T, the transmission coefficient for a Rayleigh wave around a 90^o corner, from the reflection factor, the following formula is used:

$$T = 1 - R \quad (7)$$

Omitting any conversion to other wave types. The power transmission, which is the relevant quantity for the SEA-analyis, is found by using the following formula:

$$T_{power} = 1 - |R|^2 \quad (8)$$

2.8 Statistical Energy Analysis - SEA

The method called **Statistical Energy Analysis**, **SEA**, uses the statistics of a system of a number of modes, to look upon the properties of vibrations in it [5]. Originally, this method was applied for room acoustics, and later for plates. A few of these model results were completed as far back as 1953 by Shröder. If a system has a given response in every *position* and for each *frequency*, the total response is calculated from the summation of these modes having a *random phase*, and a relatively similar distribution of energy between the modes. This will be a good approximation, for a number of *dynamical systems*, above a specific limit called the **critical frequency**.

If using SEA to calculate the response of a resonant system, four steps are used [6]:

1. A model of the dynamical system with respect to **sub-systems** and **coupling interfaces**.
2. Finding the parameters required to build the model.
3. Calculating the distribution of energy between the sub-systems included in the model.
4. Calculating the **levels of response** of the sub-systems.

It is hard work to make a model of SEA, that reflects reality [6]. There are several software that can do the calculations, but the result is also dependent on the personal knowledge and previous work in the field. The experiment is used to verify the model. This can for example be a measurement of the radiated sound power from a solid, compared to data from the model. This is important for finding errors and application limits of the model.

An SEA-model basically gives the **energy flow** and **vibrational energy accumulation** in an advanced, real object that posess both acoustic and structural properties (**vibro-acoustic system**) [6]. Energy is stored inside the sub-systems, which have different modal and structural properties. Normally, one type of mode is present in each sub-system (e.g. longitudinal, shear, Rayleigh etc.), and can co-exist with each other as different sub-systems. The different types of modes are normally bounded from each other by a discontinuity, between the sub-systems. It is often possible to find these different sub-systems , also if the system are made up of several structural and acoustic parts. Only the energy found in the resonances is of concern, used in the **expressions for the power flow**. The responses of a system that is largely damped is normally estimated to be too low, because the non-resonant response is not included. There is, although, a suggestion from Maidanik [14], [15], that the SEA-analysis can take into account the non-resonant field in the sub-systems. This will although make the model more complicated. The assumption of **conservative coupling** is also useless with this formulation.

In the study of a number of different modes, the importance is that they meet the conditions of *equality* and *dependence* [6].

- **Equality** means that all the modes of the sub-system studied has almost similar excitation of force, coupling losses to adjacent sub-systems, and losses in the material. If these characteristics are fulfilled, the modes will have almost similar vibrational energy, and this theory is then valid.
- **Dependence** means that the modes have an impact upon the internal losses, transmission and/or storage of energy in the system. If a group of modes that are not really relevant, are included in the model, the analyze may be more complicated than necessary.

The sub-systems that are included in the model are **elastic and linear structures** of certain size, or **acoustic cavities**. These different sub-systems are expressed each by their **specific vibrational modes** and their **internal losses**. The energy is either [6]:

1. **Lost** by the damping of the material
2. **Transmitted** to another sub-system

It is possible to implement some basic suppositions, and therefore widen the analyze of the flow of energy from a couple of resonators to a couple of bundles of resonators (sub-systems).

The following properties of the system are assumed [6]:

- The resonators in the 1st sub-system have **weak coupling** to the resonators of the 2nd sub-system.
- The general forces of modes must be **non-correlated**.
- The **natural frequencies** of the sub-systems have the same chance of occurrence in a frequency band $\Delta\omega$.
- The resonators of a sub-system have **equal energies**.
- The full energy description of a sub-system is the total contribution from each mode being resonant, and no non-resonant energy is taken into account.

Weak coupling does not have to state that there is a weak physical coupling in-between two of the sub-systems. The weak coupling phenomena is valid in case that the power that is transferred between two sub-systems are considerably smaller than the internal losses in the transferring sub-system. Large **internal losses** and large **reflection** at the coupling interfaces, and big **differences in wave impedances** will contribute to this.

2.8.1 Lower limit of applicability - SEA

In order to use the method of SEA, it is assumed that the wavelength of the waves traveling in the medium is short in comparison to the dimensions of the object. This means that there is a lower limit of applicability for SEA, that is generally used in order to have a working sub-system. The formula that is used to calculate the lower limit of applicability for the SEA analysis is given by [5]:

$M = \eta \cdot f \cdot n(f) > 1$

in which:

η is the loss factor, $n(f)$ is the modal density, f is the frequency.

2.8.2 Parameters needed for an SEA-model

The parameters needed to establish the SEA model are the following [6]:

- ***Input powers***, W_i, into the i-th sub-system
- ***Modal densities***, n_i, for the i-th sub-system
- ***Internal loss factors***, η_i, for the i-th sub-system
- ***Coupling loss factors***, η_{ij}, for the connection between the i-th and j-th sub-system

2.8.3 Input power

The input power is found by the external force doing work on the system, giving it a power input. If it is known, it can be used directly. It can also be calculated, if the force doing work on the system is known (assumed that the data for the sub-systems are known) [6]. It could e.g. be a **point force** acting on the object in 2D, or an **acoustic reverberant field** acting on the object in 3D. It could also be a **percussive force** working in a solid medium (e.g. a **rock drill**), giving it an input power of a certain amplitude.

2.8.4 Modal density

The **modal density** is defined as the quota of the number of *modes* and the *bandwidth* of the part of the frequency domain studied. It is generally described as [6]:

$n_i(f) = \frac{\Delta N}{\Delta f}$

in which ΔN is the number of modes in a frequency band Δf.

It can be estimated from formulas, or found in literature, for common objects, given e.g. in [7] or [8].

It is estmated as (1D subsystem - beam or rod):

$$n(f) = \frac{2 \cdot L}{c_g} \quad (1)$$

where L is the length of the interface of coupling, and c_g is the group velocity.

It is estimated as (2D plates):

$$n(f) = \frac{A \cdot \omega}{c_p \cdot c_g} + \frac{P}{c_g} \quad (2)$$

where A is the area of the plate, ω is the angular frequency, c_p is the phase velocity, and P is the full perimeter of the plate surfaces.

It is estimated as (3D cavity):

$$n(f) = \frac{\omega^2 \cdot V}{\pi \cdot {c_l}^2 \cdot c_g} + \frac{A \cdot \omega}{c_l \cdot c_g} + \frac{P}{c_g} \quad (3)$$

where V is the volume of the 3D cavity, A is the area of the cavity sides, and P is the full perimeter of the cavity sides.

It is possible to find the modal densities (the mean of how many modes exist per Hz or radian), from computations in the SEA-software [6].

It has the unit [1/Hz]. This means, that the considered structure, is seen as several different *resonators* of which the *energy* is summed up to obtain the full *energy* doing work on the structure.

2.8.5 T60

The reverberation time, T60, is defined by [20]:

$$T60 = \frac{2.2}{f_0 \eta_i} \quad (1)$$

in which f_0 is the resonance frequency of the structure, and η_i is the internal loss factor of the structure.

This equation can be modified to produce:

$$\eta_i = \frac{2.2}{f_0 T60} \quad (2)$$

The T60 is a measure of how long it takes for the vibrational level to drop by 60 dB.

2.8.6 Internal loss factors

The energy losses, meaning how much energy is lost mainly due to damping in each of the **sub-systems**, are denoted as [6]:

$$\eta_i = \frac{\Pi_{i,diss}}{\omega E_i} \quad (1)$$

in which $\Pi_{i,diss}$ is the power being lost in the i-th sub-system, and E_i is the energy of vibrations being accumulated in the i-th sub-system.

The above described formulas describe the quantity of internal losses, related to

the elastic energy being accumulated in each sub-system. These data, for each sub-system, has to be given by material data sheets, or estimated in the form of **loss factors** of an object being damped [9].

2.8.7 Coupling loss factors

The power flow from one of the subsystems to another one is formulated by the **coupling loss factors** (CLF:s), η_{ij}, in the equation [6]:

$$\eta_{ij} = \frac{\Pi_{ij}}{\omega E_i}$$

in which Π_{ij} denotes the flow of power between the i-th subsystem and the j-th subsystem, and E_i is the sum of energy which is accumulated in the i-th subsystem, if $E_j = 0$.

The CLF:s are dependent upon certain properties of coupling interfaces [7]. The CLF:s can be found from the transmission loss of a solid media located between different acoustic cavities. If the case of coupling between a structural sub-system, and an acoustic sub-system, is studied, the CLF:s can be found from the radiation efficiency or the radiation resistance. If looking at an interface between sub-systems having the form of plates, the CLF:s are dependent on the wave transmission coefficients of the coupling interface being studied. If a coupling is a point connection, the CLF:s can be obtained from the mechanical mobilities of the sub-systems being coupled to it. The CLF:s for a certain path where the energy is transferred, can be found from literature [7], [8] and [10].

The coupling loss factors for a 2D type structure is found as [4]:

$$\eta_{ij} = \bar{\tau_{ij}} \frac{c_g}{\omega} \frac{l_c}{\pi S_v} \quad (1)$$

and for a 3D type structure it is found as:

$$\eta_{ij} = \bar{\tau_{ij}} \frac{c_g}{\omega} \frac{S_c}{4V_v} \quad (2)$$

in which $\bar{\tau_{ij}}$ is the mean transmission coefficient over the total number of incidence angles, l_C is denoted as the length of the junction separating both sub-systems, S_V is the area of the 'transferring' sub-system, S_C is the area of the junction, and V_V is the volume that the 'transferring' structure has.

2.8.8 Power flow equations

In the methodology of SEA, the relationship of **energy flow** between the sub-systems can be found from the formulas below. The relationships of the power flow between the different sub-systems are shown in figure 15.

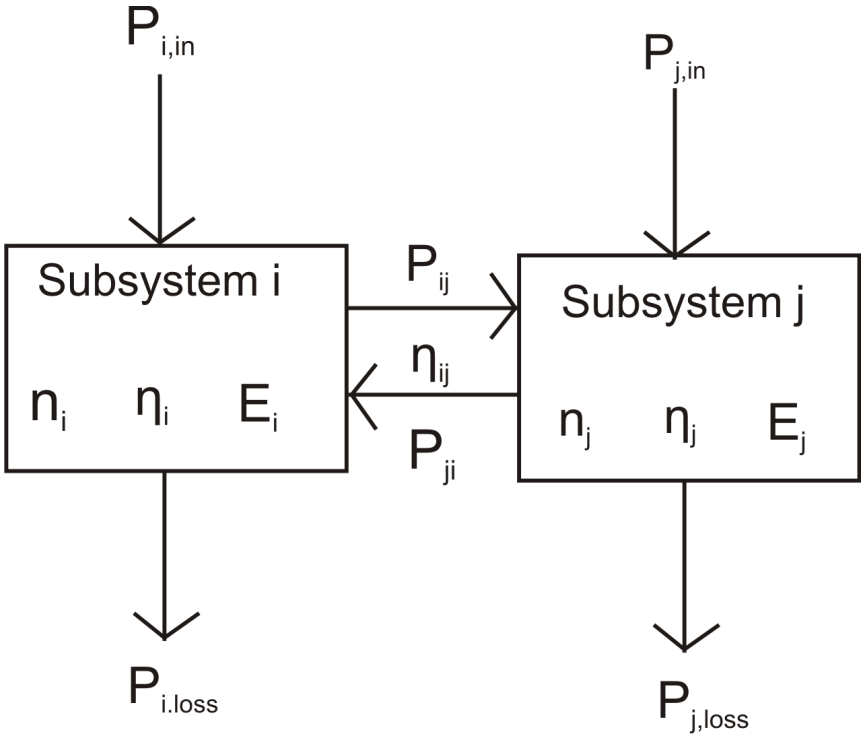

Figure 15: The power flow between two different sub-systems. [11]

The equations used to describe the power flow are the following [11]:

Sub-system i: $P_{i,in} + P_{ji} = P_{i,loss} + P_{ij}$ (1)
Sub-system j: $P_{j,in} + P_{ij} = P_{j,loss} + P_{ji}$ (2)

where the internal losses, P_{li}, are given by:

$P_{li} = \omega \eta_i E_i$ (3)

And the transmitted powers, P_{ij}, are given by:

$P_{ij} = -P_{ji} = P'_{ij} - P'_{ji}$ (4)
$P'_{ij} = \omega \eta_{ij} E_i$ (5)
$P'_{ji} = \omega \eta_{ji} E_j$ (6)

where η_{ij} and η_{ji} are the CLF:s, that fulfill the relationship:

$\eta_{ij} n_i = \eta_{ji} n_j$ (7)

this gives the power transmission, P_{ij}, to be expressed by:

$P_{ij} = \omega \eta_{ij} (n_j E_i - n_i E_j) = \omega \eta_{ij} n_i (\frac{E_i}{n_i} - \frac{E_j}{n_j})$ (8)

following the expression above, the power flow in eq. (1) and (2) can be expressed by:

$$P_{i,in} = \omega\eta_i E_i = \omega\eta_{ij} n_i (\frac{E_i}{n_i} - \frac{E_j}{n_j}) \quad (9)$$

$$P_{j,in} = \omega\eta_j E_j = \omega\eta_{ji} n_j (\frac{E_j}{n_j} - \frac{E_i}{n_i}) \quad (10)$$

From this equation, the energy balance for each sub-system can be calculated, if the parameters of the SEA calculations: the modal density, internal loss factor, coupling loss factor, and input power, are known.

2.8.9 Computation of the energy distribution

The "stationary" energy levels for each sub-system, can simply be found from the given energy balance equations, e.g. the levels of response for pressure, acceleration, and stress [6]. If the parameters used for sub-systems, and coupling interfaces, are known, the below matrix equation can be used:

$$\Delta f \cdot \omega[A] \cdot \{E_m\} = \{W_{in}\}$$

In the matrix above, A will have real values, have symmetry, always be positive, and of size NxN, in which N is the number of subsystems. By denoting the different sub-systems by numbers, the matrix can be solved as a version which is simplified, which will allow a faster calculation, and give the opportunity to include more sub-systems [6].

For a system built up of several different modes (as described in previous section), this matrix will be described by:

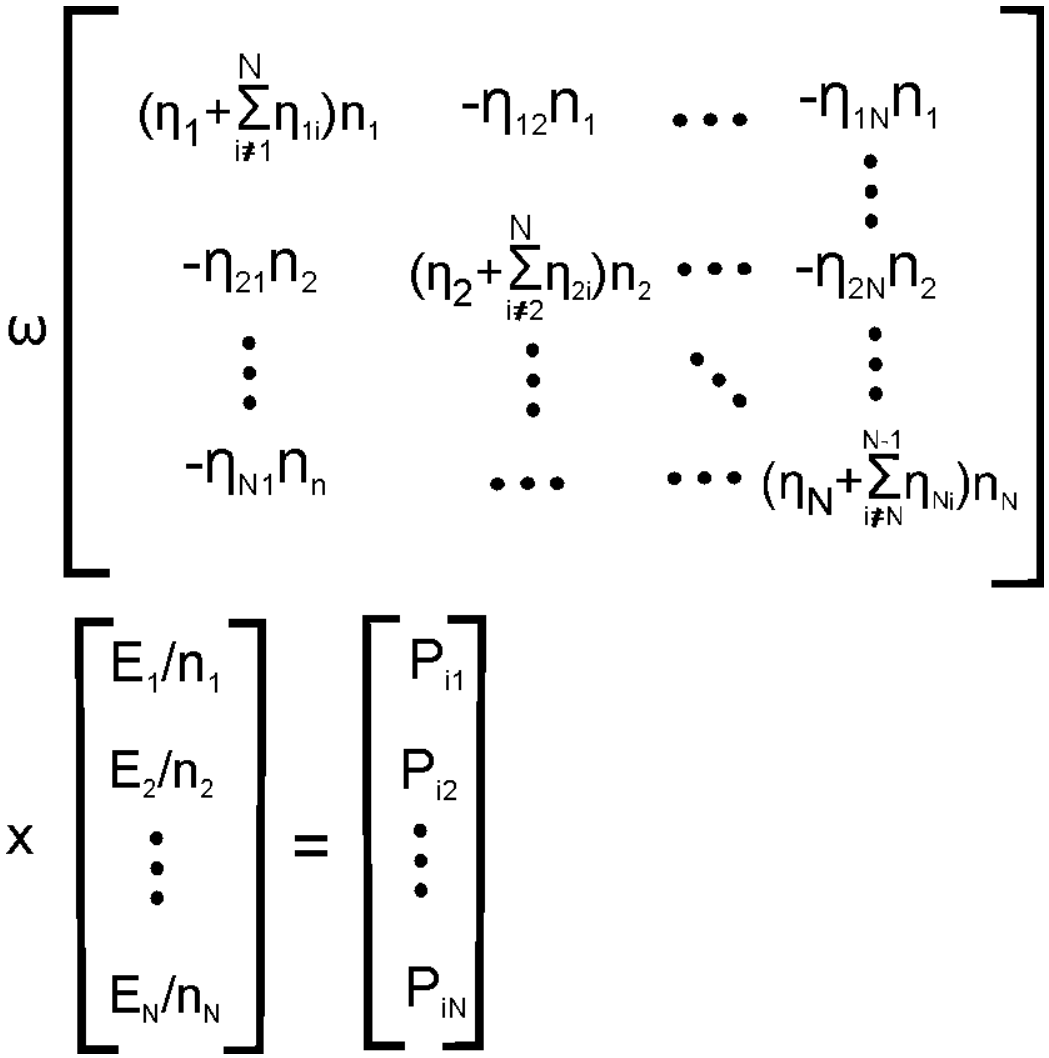

Figure 16: The power flow between many different sub-systems. [11]

2.8.10 Computation of the response levels

The total energy, in each sub-system, can be found from a multiplication of the calculated modal energy levels, with the estimated number of modes in each 3rd-octave band. Looking at the total energy in each of the bands, the average response amplitudes are estimated. In the case of an **acoustic subsystem** which is a 3D cavity, the spatial average of the sound pressure is:

$$E = \frac{\langle p^2 \rangle}{\rho c^2} V$$

it is also found, that there is a relation between the total energy in a sub-system of a structure and the average vibration velocity over the space:

$$E = M\langle v^2 \rangle$$

where M is denoted as the total mass of the sub-system.

2.9 Excitation of different waves

There is a problem to determine the distribution of the different wave types, which are excited, when launching the excitation with a point-source. If a surface source is used, one can expect, from previous studies in the field, that the main contribution to the field of waves will be in form of surface waves, confined to the surface of the cylinder, and to some extent, extending into the interior of the cylinder. The rest of the energy, one can expect, will form volume waves in the interior of the cylinder. This problem is illustrated in figure 17. This distribution, according to [17], will be approximately 67 % into surface waves, 26 % into shear waves, and 7 % into longitudinal waves, for a Poisson's number of $\nu = 0.25$. In [30], this analysis is done in greater detail, giving the distribution between wave types, for a point excitation on a half-infinite solid.

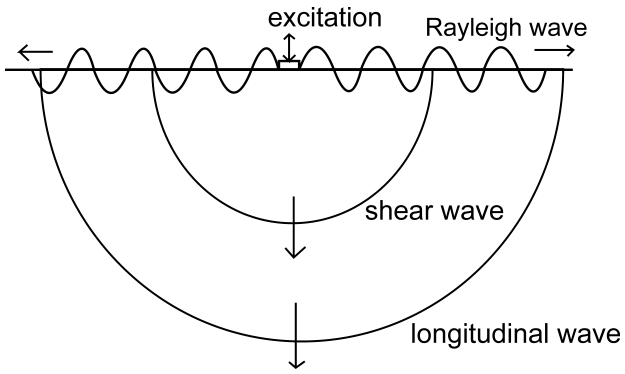

Figure 17: The problem of a single surface-source excitation of a half-infinite solid medium. [17]

Longitudinal and shear waves. A round disk, of radii a, is vibrating in normal direction on the surface of the solid, in figure 18. This media is half-infinite and isotropic. This motion is giving a stress beneath the disk, at time t, expressed by $P_0 e^{j\omega t}$. Here, P_0 and ω are positive constants [30]. The longitudinal and shear waves propagates in a spherical pattern. The interesting part is to find the intensity of these waves. Therefore, it is suitable to introduce a system of spherical coordinates (R, θ, ϕ), in which the origo is located at the mid-point of the disk, at time $t = 0$. The polar angle θ is zero at points inside the medium, on the axle of the disk.

The radial and shear parts of the displacement, u, can be described by u_R and u_θ, respectively, and we find the equations:

$$u_R \approx -\frac{a^2 P_0}{2c_{44}} \frac{e^{(j\omega t - k_l R)}}{R} \Theta_1(\theta) \quad (1)$$

$$u_\theta \approx -\frac{ja^2 \mu^3}{2c_{44}} \frac{e^{j(\omega t - k_t R)}}{R} \Theta_2(\theta) \quad (2)$$

for big R and small a, in which

$$\Theta_1(\theta) = \frac{\cos\theta(\mu^2 - 2\sin^2\theta)}{F_0(\sin\theta)}, \; \Theta_2(\theta) = \frac{\sin 2\theta \sqrt{\mu^2 \sin^2\theta - 1}}{F_0(\mu \sin\theta)}$$

$$F_0(\zeta) = (2\zeta^2 - \mu^2)^2 - 4\zeta^2\sqrt{\zeta^2 - \mu^2}\sqrt{\zeta^2 - 1}$$

$k_l = \omega\sqrt{\rho/c_{11}}$, $k_t = \omega\sqrt{\rho/c_{44}}$,

and

$$\mu = \sqrt{c_{11}/c_{44}} = k_t/k_l = \sqrt{2(1-\nu)/(1-2\nu)}$$

in which c_{11} and c_{44} are the constants of elasticity for compressive, and transverse motion, ζ is an integrand, ν is the Poisson's ratio, and ρ is the density of the medium.

The intensity of a transverse or longitudinal wave can be expressed by the amount of each wave type, being radiated from the excitation. This is described in terms of power per unit area, over time, of the given wave surface:

$\Gamma_l = -\frac{1}{2}\dot{u_R}\widehat{RR*}$, $\Gamma_s = -\frac{1}{2}\dot{u_\theta}\widehat{R\theta*}$,

for each case, in which the * means the conjugate complex.

The radial and transverse stress parts, over the surface of the wave, $\widehat{RR}$ and $\widehat{R\theta}$, and the parts of displacements, are related by the formulas:

$$\widehat{RR} = c_{12}\nabla.\mathbf{u} + 2c_{44}\frac{\partial u_R}{\partial R},\ \widehat{R\theta} = c_{44}R\frac{\partial}{\partial R}(\frac{u_\theta}{R}) + \frac{1}{R}\frac{\partial u_R}{\partial \theta},$$

in which $c_{12} = c_{11} - 2c_{44}$, by regular description. The expressions (1) and (2) gives another formulation of these stresses:

$$\widehat{RR} \approx \frac{ja^2k_l\mu^2P_0\Theta_1(\theta)}{2R}e^{j(\omega t - k_lR)},\ \widehat{R\theta} \approx -\frac{a^2k_l\mu^4P_0\Theta_2(\theta)}{2R}e^{j(\omega t - k_tR)},$$

The oscillation frequency can be denoted by f_v and the velocity of longitudial waves in the medium by v_l, so that:

$f_v = \omega/2\pi$, $v_l = \omega/k_l$,

thus, the intensities of longitudinal waves and shear waves are found as:

$$\Gamma_l \approx \frac{\pi^2 f_v^2 a^4 \mu^4 P_0^2}{2\rho {v_l}^3}\frac{\Theta_1(\theta)}{2}R^2,$$

$$\Gamma_t \approx \frac{\pi^2 f_v^2 a^2 \mu^9 P_0^2}{2\rho {v_l}^3}\frac{\Theta_2(\theta)\Theta_2^*(\theta)}{R^2},$$

and it is important to note that $\Theta_1(\theta)$ is real valued.

W_l and W_t will subsequently be used to describe the power being radiated in both longitudinal and shear waves. After this, it is possible to perform an integration of the intensities over a half sphere having big radius R, and end up with:

$$W_l = \frac{\pi^3 f_v^2 a^4 \mu^4 P_0^2}{\rho {v_l}^3}\int_0^{\pi/2}\Theta_1(\theta)^2\sin\theta d\theta, \quad (3)$$

$$W_t = \frac{\pi^3 f_v^2 a^4 \mu^9 P_0^2}{\rho {v_l}^3}\int_0^{\pi/2}\Theta_2(\theta)\Theta_2^*(\theta) sin\theta d\theta \quad (4)$$

The preceeding integrals have been calculated, for a value of $\mu = \sqrt{3}$, leading to a Poisson's ratio of 0.25, and the result is [17]:

$W_l = 0.333\frac{\pi^3 f_v^2 a^4 P_0^2}{\rho v_l^3}$, $W_s = 1.246\frac{\pi^3 f_v^2 a^4 P_0^2}{\rho v_l^3}$

Surface waves. It is also of interest to find how much power is being distributed into the surface wave. For this purpose, a system of coordinates in the shape of a cylinder, (r, ϕ, z), is used, where the plus z-axis is interfering with the line $\theta = 0$, in the spherical coordinate system described earlier in this chapter [17]. The mean intensity is then found from:

$\Gamma_{ray} = -\frac{1}{2}\dot{u_z}\widehat{zr}^* - \frac{1}{2}\dot{u_r}\widehat{rr}^*$.

The Rayleigh wave has displacement parts both radially, along the coordinate r, and in z direction. These displacement parts can be found by looking at the integrals of the overall parts of displacement, and observing how much a pole of the integrand, will affect the result of each integral. This pole is found at the position $\zeta = -p$ on the minus real axis, in which p, is given as the plus root of eq. $F_0(\zeta) = 0$. The term $F_0(\zeta) = 0$ is depending on Poisson's ratio of the medium. The parts of the displacement field are given by:

$$u_z \approx \frac{a^2 e^{-\frac{1}{4}j\pi} P_0}{c_{44} F_0'(p)} \sqrt{\frac{\pi k_1 p(p^2-1)}{2r}} e^{j(\omega t - k_1 pr)} \{2p^2 e_\mu - (2p^2 e_\mu - (2p^2-\mu^2)e_1\}, \quad (5)$$

$$u_r \approx \frac{a^2 e^{\frac{1}{4}j\pi} P_0}{c_{44} F_0'(p)} \sqrt{\frac{\pi k_1 p^3}{2r}} e^{j(\omega t - k_1 pr)} \{2\sqrt{p^2-1}\sqrt{p^2-\mu^2} e_\mu - (2p^2-\mu^2)e_1\} \quad (6)$$

in which $e_\mu = \exp\{-k_1 z\sqrt{p^2-\mu^2}\}$, $e_1 = \exp\{-k_1 z\sqrt{p^2-1}\}$

The stress parts, which are relevant, are given in terms of the displacement parts u_z and u_r by:

$\widehat{zr} = c_{44}(\frac{\partial u_z}{\partial r} + \frac{\partial u_r}{\partial z})$, $\widehat{rr} = c_{12}\nabla.\mathbf{u} + 2c_{44}\frac{\partial u_r}{\partial r}$.

The right parts of the equations above, can be replaced by the asymptotic expressions that was found by differentiation of (5) and (6), and usage of the relation $F_0(p) = 0$. This will give the following expressions:

$$\widehat{zr} \approx \frac{-a^2 P_0}{F_0'(p)} \sqrt{\frac{\pi k_1^3 p^3 (p^2-1)}{2r}} 2(2p^2-\mu^2)\{e_\mu - e_1\} e^{j(\omega t - k_1 pr + \frac{1}{4})},$$

$$\widehat{rr} \approx \frac{a^2 P_0}{F_0'(p)\sqrt{\frac{\pi k_1^3 p}{2r}}\{(2p^2-\mu^2)e_\mu - (2p^2+\mu^2-2)e_1\} e^{j(\omega t - k_1 pr - \frac{1}{4}\pi)}}.$$

Subsequently, the mean intensity of the Rayleigh wave will be:

$$\Gamma_{ray} = \frac{\omega {k_1}^2 a^4 P_0^2}{2c_{44} r} X(k_1 z) = \frac{2\pi^2 f_v^2 a^4 \mu^2 P_0^2 k_1}{\rho v_l^3 r} X(k_1 z)$$

in which:

$X(k_1 z) = \frac{\pi(2p^2-\mu^2)}{4\{F_0'(p)\}^2}[4p^2(p^2-1)\{2p^2 e_\mu - (2p^2-\mu^2)e_1\}(e_\mu - e_1) + (2p^2-\mu^2)\{(2p^2-\mu^2)\{(2p^2-\mu^2)e_\mu - 2p^2 e_1\}\{(2p^2-\mu^2)e_\mu - (2p^2+\mu^2-2)e_1\}]$,

It is also possible to integrate this expression over a large cylinder, having a large radius r. This integration will lead to the the following formula, describing the radiated power of the Rayleigh wave:

$$W_{ray} = \frac{4\pi^3 f_v^2 a^4 \mu^2 P_0^2}{\rho v_l^3} \int_0^\infty X(k_1 z) d(k_1 z). \quad (7)$$

Integral (7) can be expressed by doing a summation of the functions e_μ^2, $e_\mu e_1$ and e_1^2, and if one assign numbered values to the coefficients and the exponents, it's no big deal to evaluate the integral. If the term p is known, the variable $F_0'(p)$ can be expressed by:

$$F_0'(p) = 8p\{(2p^2 - \mu^2) - \frac{(2p^2-\mu^2)^2}{4p^2} - \frac{2p^4(2p^2-\mu^2-1)}{2p^2-\mu^2)^2}\}.$$

For the case of $\mu = \sqrt{3}$, the value of p will be:

$$p = \frac{3}{2}\sqrt{1 - \frac{1}{\sqrt{3}}} = 1.8839,\ F_0'(p) = -8\sqrt{3}p = -26.104$$

and subsequently $X(k_1 z) = 1.5383 e_\mu^3 - 3.1192 e_\mu e_1 + 1.8131 e_1^2$

in which $e_\mu = \exp(-0.7410 k_1 z)$, $e_1 = \exp -1.5966 k_1 z$

and if this formulation is placed in (7), we get [17]:

$$W_{ray} = 3.257 \frac{\pi^2 f_v^2 a^4 P_0^2}{\rho v_l^3}$$

At last, the full power being generated by the point-force excitation, is obtained by merging eq. (3), (4) and (7):

$$W = W_l + W_s + W_{ray} = 4.836 \frac{p i^3 f_v^2 a^4 P_0^2}{\rho v_l}.$$

2.10 Euler-Bernoulli theory

The Euler-Bernoulli theory, and wave approach, are described in detail in [24]. These theories are used to calculate the parameters of waves moving in a beam-like object.

It is assumed that we have a longitudinal wave incident on the end of a beam. The reflected wave will also be longitudinal. We assume that the end of the beam is a free surface, meaning that the force that is acting on this end is zero. The wave being incident can be described by:

$$\xi_i(x,t) = \xi_i(\omega) e^{-jkx} e^{j\omega t} \quad (1)$$

where $\xi_i(\omega)$ is the complex amplitude of the wave. The wave which is reflected will have a proportional amplitude, in relation to the incident wave. The reflected wave is defined as:

$$\xi_r(x,t) = r\xi_i(\omega) e^{jkx} e^{j\omega t} \quad (2)$$

where r is the reflection factor, which is complex.

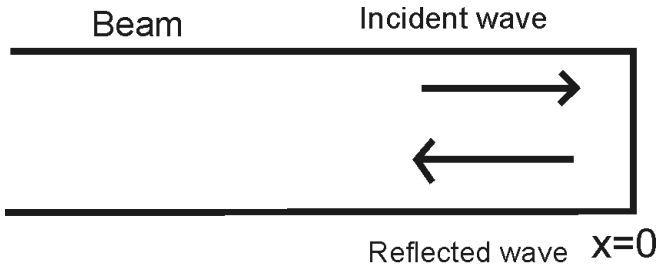

Figure 18: A longitudinal wave moving in a beam, and being reflected at the end of the beam.

A longitudinal wave moving through the beam, being reflected at the end of the beam, is shown in figure 18.

The displacement of the beam can be seen as a superposition of both waves [24]:

$\xi(x,t) = \xi_i(\omega)(e^{-jkx} + re^{jkx})e^{j\omega t}$ (3)

And the force and the displacement are related by hooke's law:

$F(x,t) = -ES\frac{\partial\xi(x,t)}{\partial x}$ (4)

in which E is the young's modulus, and S is the cross-sectional area of the beam. which will give, together with eq. (3):

$F(x,t) = jkES\xi_i(\omega)(e^{-jkx} - re^{jkx})e^{j\omega t}$ (5)

At x=0, the boundary condition is:

$F(x=0,t) = jkES\xi_i(\omega)(1-r)e^{j\omega t} = 0$ (6)

which is only true when r=1. This means that the incident and reflected wave must have the same amplitude in order to have proper boundary conditions. The same standing wave pattern as a sound wave moving in a Kundt's tube, can be found on the beam, if measuring with an accelerometer along the half-infinite beam. There can exist different boundary conditions at the end of the beam. It can be e.g a mass or a spring attached to the beam's end, or a force working on the end. The reflection factor can be found from the impedance ratio of the medias on the respective sides of the boundary:

$r = \frac{Z_w - Z_T}{Z_w - Z_T}$ (7)

where Z_W is the wave impedance of the wave guide, and Z_T is the impedance of the stoppage. It is of interest to look at an example where the stoppage is a dense mass. The wave impedance for a longitudinal wave is $Z_W = \rho c_l S$, and the mass impedance is $Z_T = j\omega m$. The reflection factor of (7) can then be expressed as:

$r = \frac{\rho c_l S - j\omega m}{\rho c_l S + j\omega m}$ (8)

It is found, from (8), that if the mass can be seen as small relative to the wave impedance, it will have no effect, which means that the reflection factor will be 1, as it is for a free end.

The expression (8) is made up of both a real and an imaginairy part, according to:

$$\mathrm{Re}(r) = \frac{(\rho c_l S)^2 - (\omega m)^2}{(\rho c_l S)^2 + (\omega m)^2} \quad (9)$$

$$\mathrm{Im}(r) = -\frac{2\omega m \rho c_l S}{(\rho c_l S)^2 + (\omega m)^2}$$

It is of interest to describe the meaning of a dense mass, and this can be done by modifying the formula for the wave impedance, according to:

$$Z_w = \frac{\rho \lambda_l S}{2\pi}\omega \quad (10)$$

The expressions of the real and imaginary parts of the reflection factor, can then be written as:

$$\mathrm{Re}(r) = \frac{m_{\lambda/6}^2 - m^2}{m_{\lambda/6}^2 + m^2} \quad (11)$$

$$\mathrm{Im}(r) = -\frac{2 m_{\lambda/6} m}{m_{\lambda/6}^2 + m^2}$$

where $m_{\lambda/6} = \frac{\rho \lambda_l S}{2\pi}$

It is a frequency dependency present in eq. (11), as the wavelength of a longitudinal wave. This indicates that a mass attached to the end of the beam will affect the reflection only in case that this mass is larger than approximately 1/6 of this wavelength.

3 Measurements

In this section, measurements of the reverberation time, T60, are presented. This gives the possibility to calculate the internal loss factors, described in section 2.8.6. Also, additional measurements of the velocity, are performed for our modelling object, a cylinder of nylon. Finally, a theoretical model, described in section 2.10, is used to calculate an approximate velocity inside the cylinder.

3.1 T60 in a solid medium

In order to investigate the reverberation time, **T60**, in a solid medium, the software LMS.Test.Lab 13B, aquisition system, LMS SCADAS 20Ch, and an **accelerometer**, LMS PCB 35A16, were used. For the measurement on the cylinder of nylon, a different accelerometer was used, LMS PCB 356A12. The 1st measurement was performed on a block of **diabase**, as seen in figure 19. Both a steel hammer, a rubber hammer, and a light rubber hammer were used to excite the structure. The block was excited in a position a few decimeters from the measurement point, near the closer side of the top. The response was measured in the accelerometer position. MATLAB is used to process the results of the T60-measurements.

Figure 19: The 1st measurement taking place on a block of diabase.

It is seen from the **Energy Spectral Density** plot in LMS, in figure 20, that we have an input of energy starting at around 1.7 kHz, where the 1st resonance is located. This resonance indicates where the input of energy into the cylinder is beginning to take place.

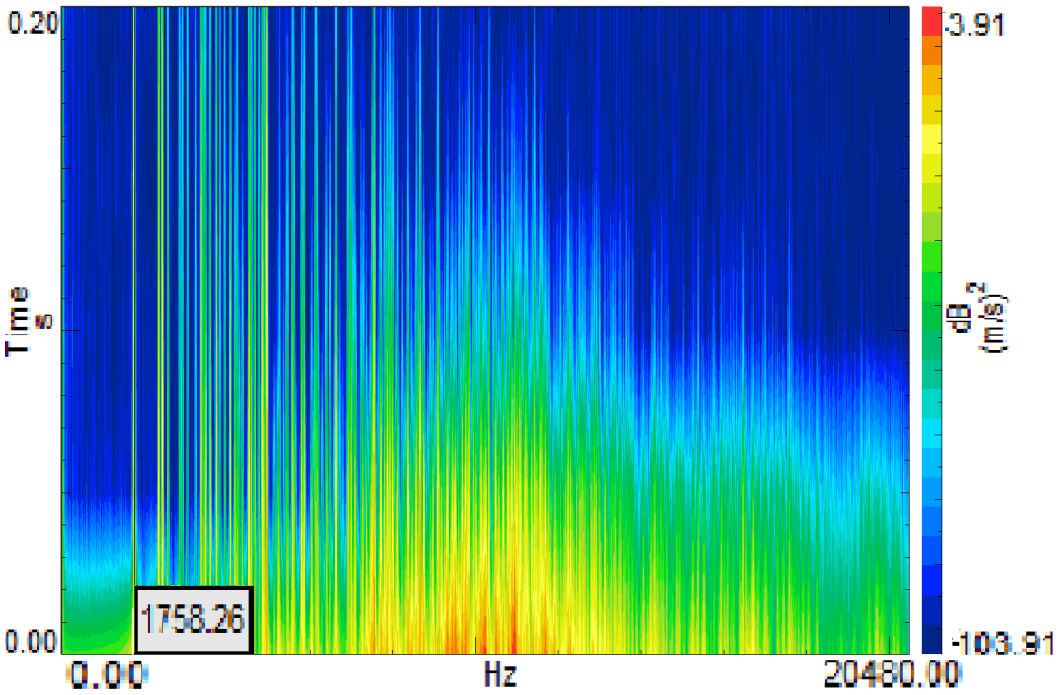

Figure 20: The Energy Spectral Density, for the block of diabase.

The results from the measurements of the T60, on the block of diabase, are shown in figure 21. The T60 for frequencies below the 1.6 kHz band are not included in this data. This is due to the fact that, as explained, we have an input of energy starting a bit above this frequency band, which would likely mean that measurements for lower frequencies are inaccurate.

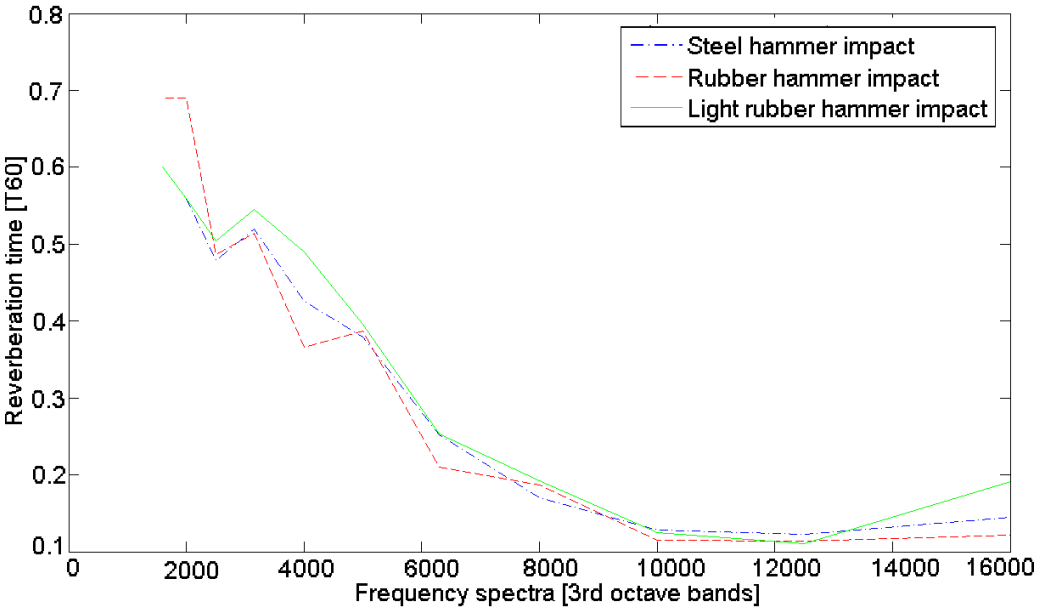

Figure 21: The results from the 1st measurement taking place on a block of diabase.

The 2nd measurement was performed on a block of steel, as seen in figure 22. The structure was excited with the types of hammers mentioned above. The area of excitation was located a few decimeters from the measurement position, near the close side of the top. The response was measured in the accelerometer position.

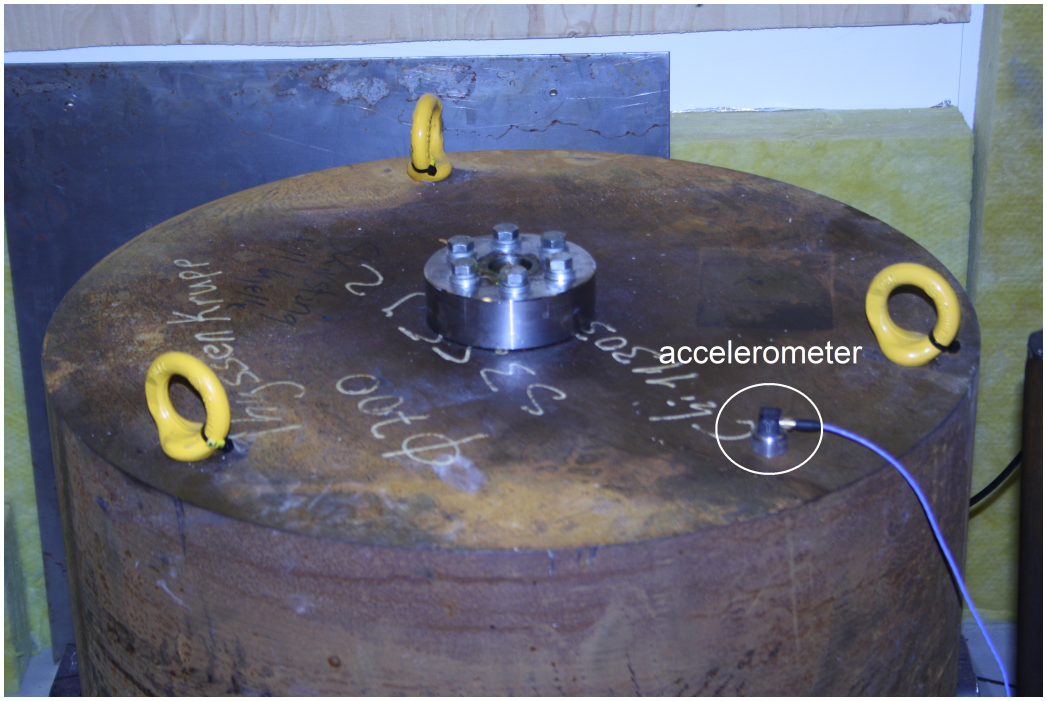

Figure 22: The 2nd measurement taking place on a block of steel.

The results of the measurement of T60, for the block of steel, is shown in figure 23.

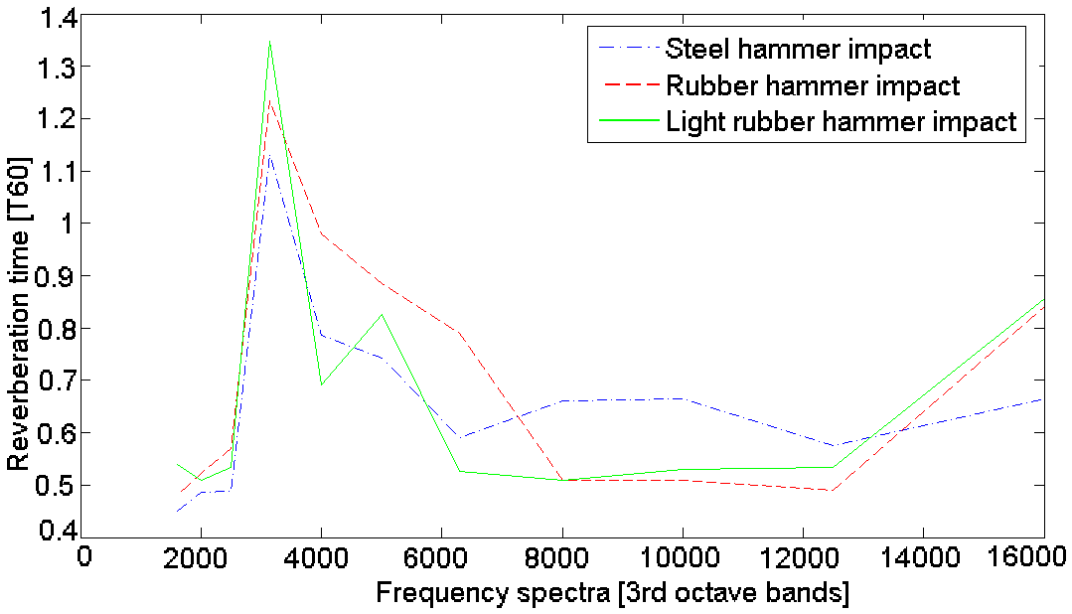

Figure 23: The results from 2nd measurement taking place on a block of steel.

The 5th measurement was performed on the cylinder of nylon, as shown in figure 24. The structure was excited using the light rubber hammer. The excitation took place close to the middle on the visible smaller side, and the response was measured with the accelerometer on the top of this side. Note: the cylinder is placed on a rubber ring. This could be mentioned as an influence on the results of the reverberation time. An alternative placement is free suspension, which could perhaps be more suitable.

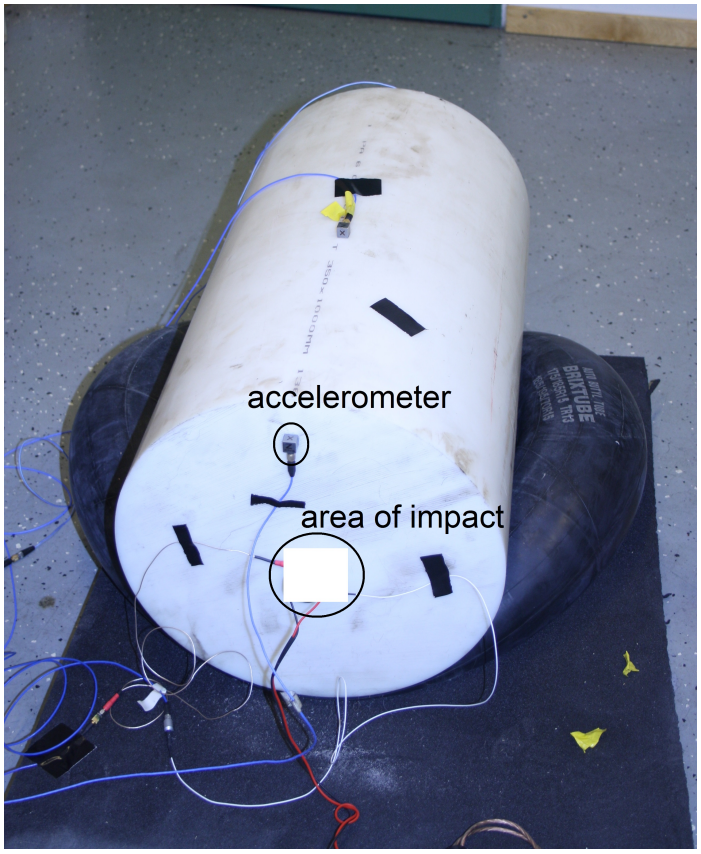

Figure 24: The 5th measurement taking place on a cylinder of nylon.

The ESD spectrum for the cylinder of nylon is given in figure 25. In this data, two peaks are found, one at around 1400 Hz, and another one at around 2100 Hz. This is likely different resonances of the cylinder, which are important for the modelling results. Also, the lower resonance indicates where we start to have an input of energy into the cylinder.

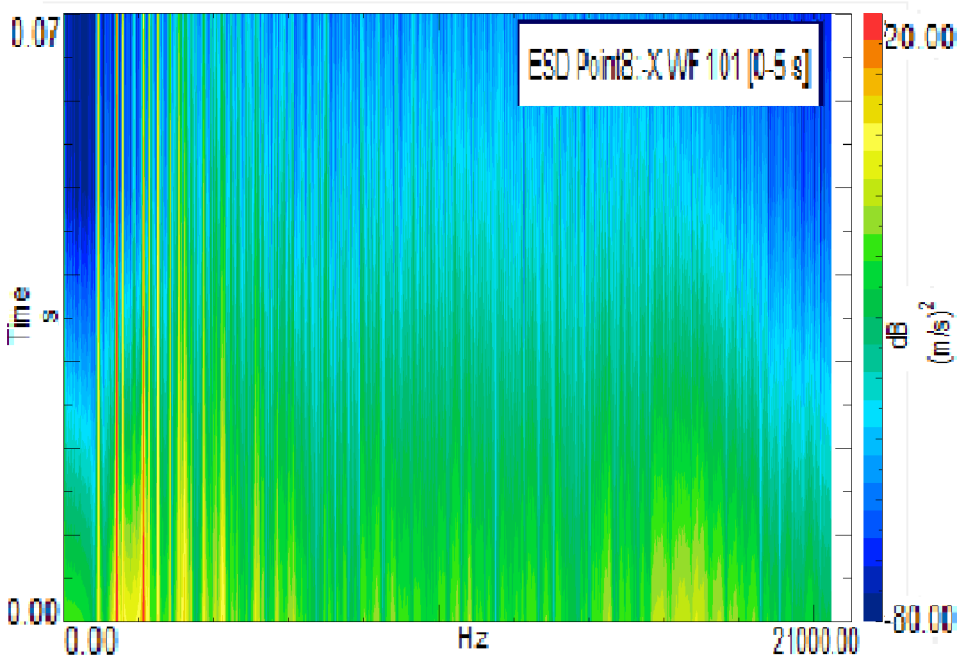

Figure 25: The ESD spectrum for the cylinder of nylon

The results from the measurement on the cylinder of nylon, are given in figure 26. The T60 for frequencies below the 2 kHz band are interpolated linearly from the value at this band. This is due to the fact that we have an input of energy starting a bit below this frequency band, as seen in the ESD-spectrum.

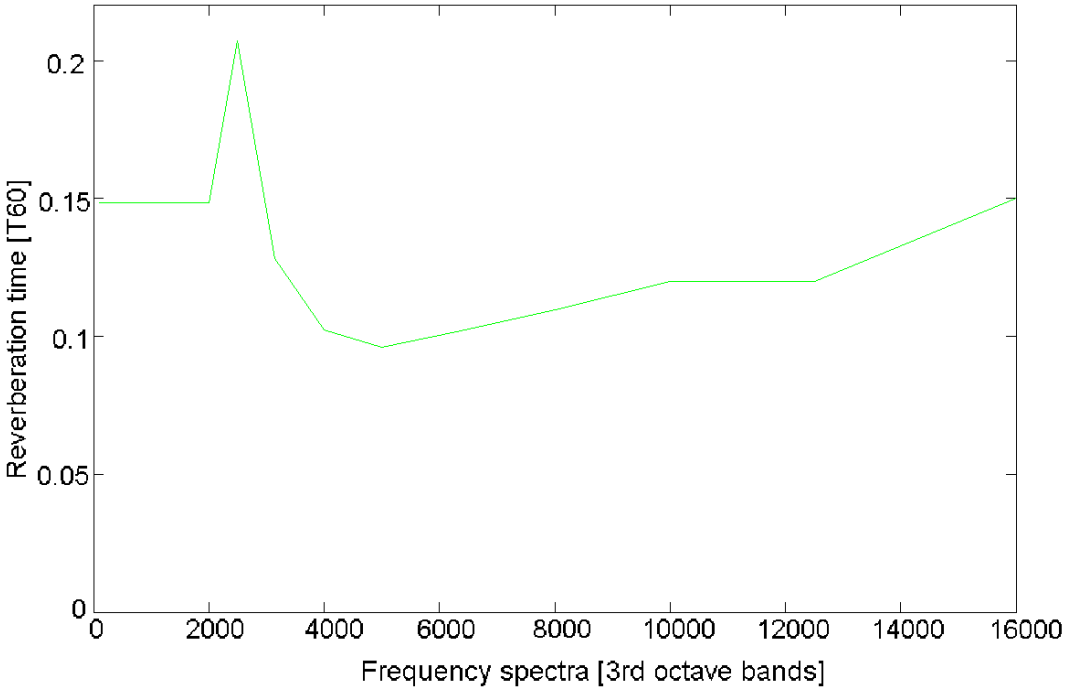

Figure 26: The results from the 5th measurement taking place on a cylinder of nylon.

3.2 Internal loss factor in a solid medium

The loss factors in this chapter, are calculated using the T60-results found in the previous section, and formula (2) of section 2.8.6. MATLAB is used to process these results.

The loss factor over the frequency bands, for the block of diabase, is shown in figure 27.

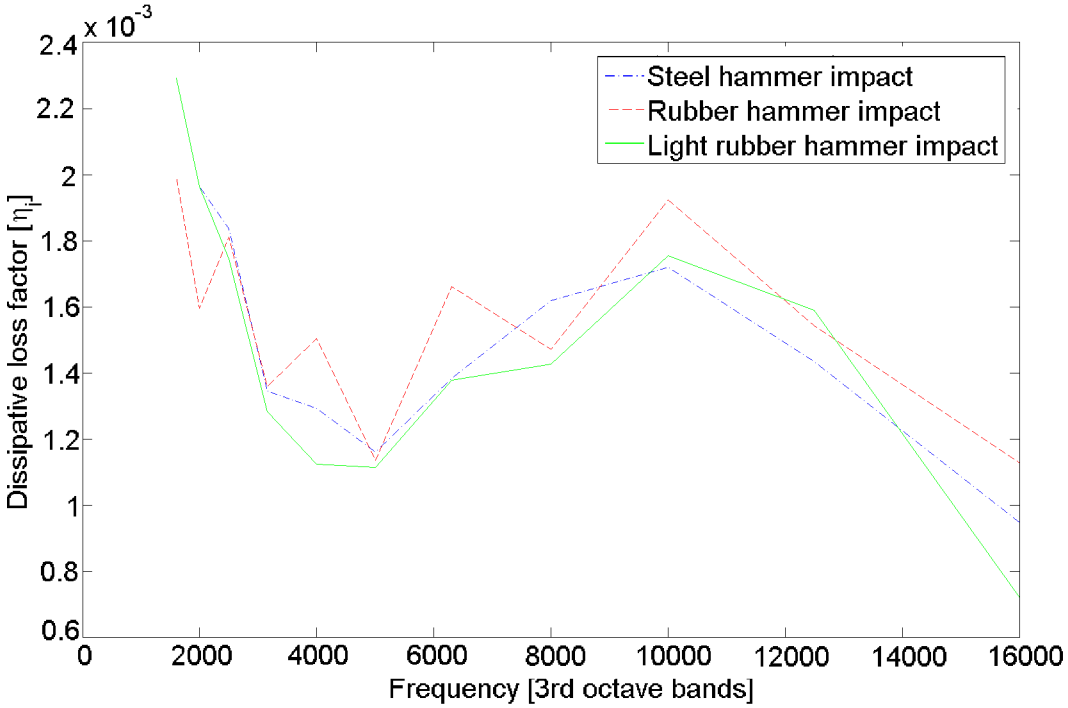

Figure 27: The internal loss factor over the frequency bands, for the block of diabase.

The loss factor over the frequency bands, for the block of steel, is shown in figure 28.

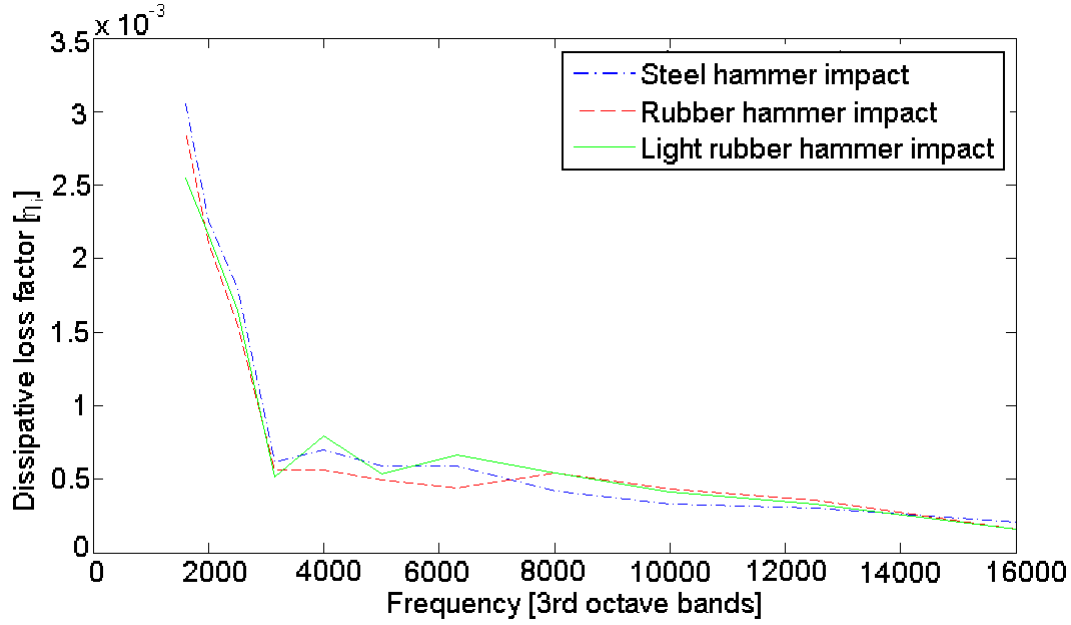

Figure 28: The internal loss factor over the frequency bands, for the block of steel.

The loss factor over the frequency bands, for the cylinder of nylon, is given in figure 29.

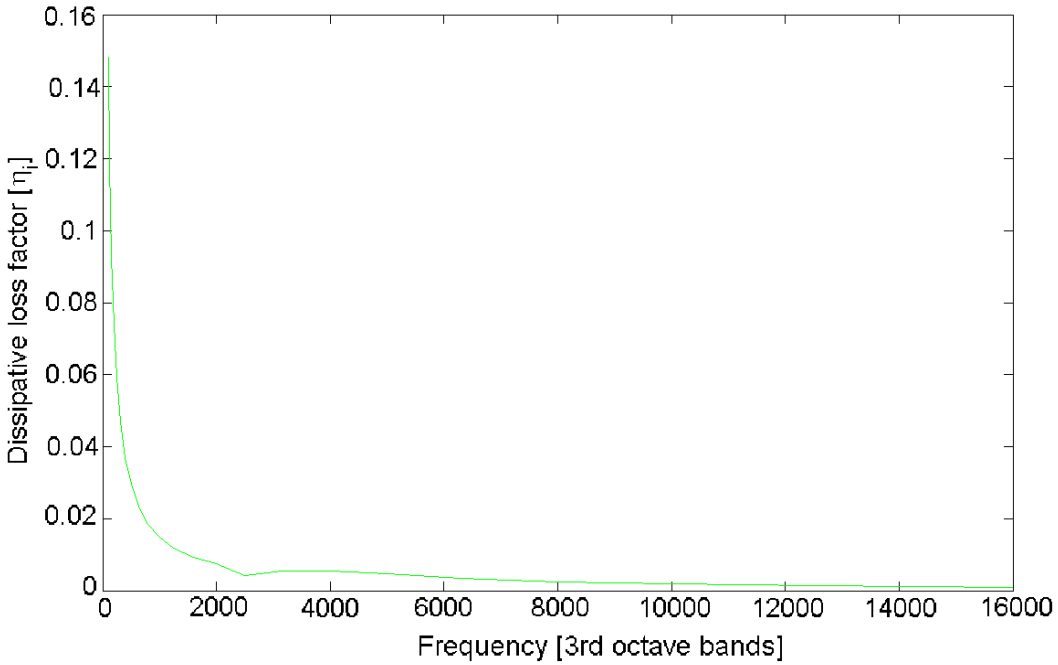

Figure 29: The internal loss factor over the frequency bands, for the cylinder of nylon.

The results of the loss factor in the cylinder of nylon, for frequencies below 2 kHz, are interpolated linearly from the value it has at this frequency. This is because the results for the T60 are not found for lower values in the measurements. This is explained in the previous section. The value of the loss factor, at 5 kHz, is 0.004575, for the cylinder of nylon.

3.3 Velocity on the cylinder of nylon

In order to find an estimation of the velocity levels of the surfaces of the cylinder of nylon, measurements were performed, after exciting the structure with a continuous excitation. The excitation of the cylinder of nylon (PA6GTECAST) was performed using a shaker, LMS Qsources Integrated miniature shaker, on the top of the cylinder (see figure 30), running at a sine of 5 kHz, and giving 1 N of input force. The accelerometers used were LMS PCB 35A36, and LMS PCB 35A12. The aquisition system used was LMS Scadas 20Ch. The data was processed in LMS.Test.Lab 13B. The response was measured in 78 different points on the surface of the cylinder + 1 stationary accelerometer, used as phase reference. This gave a total of 26 different measurements that was set up. The setup of these measurements is shown in figure 31. The animation of these velocity levels are displayed, over phase increments of 30^o, in figure 31 - 36.

Note: since the accelerometers are 3-axis, the coordinates of the measurements are referenced to the coordinate system given in figure 31 (since they may not be placed the same as the referenced coordinate system).

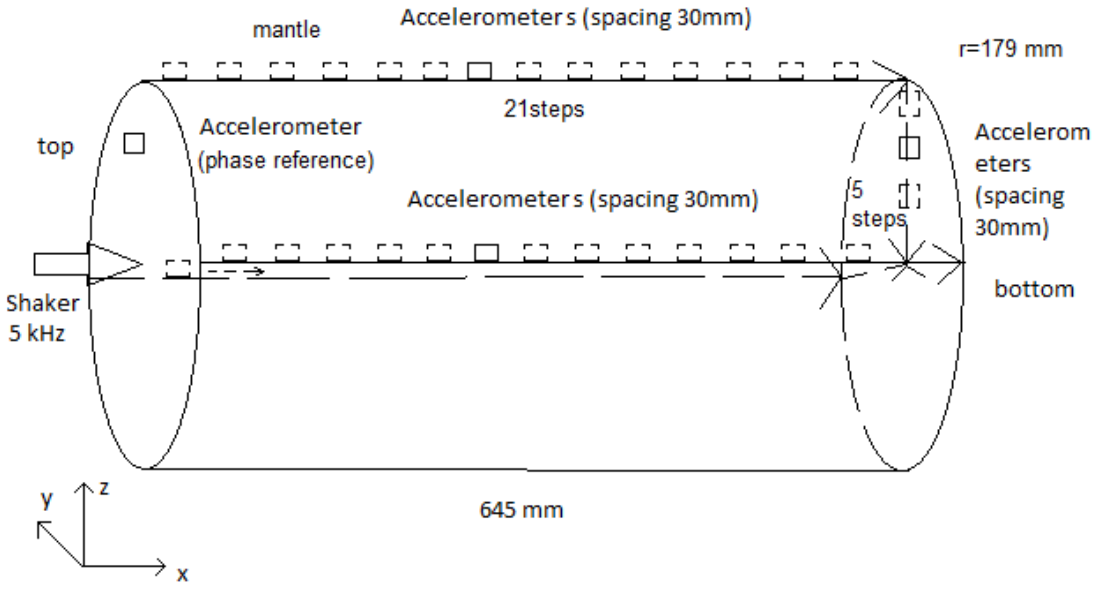

Figure 30: The measurement setup on the cylinder of nylon.

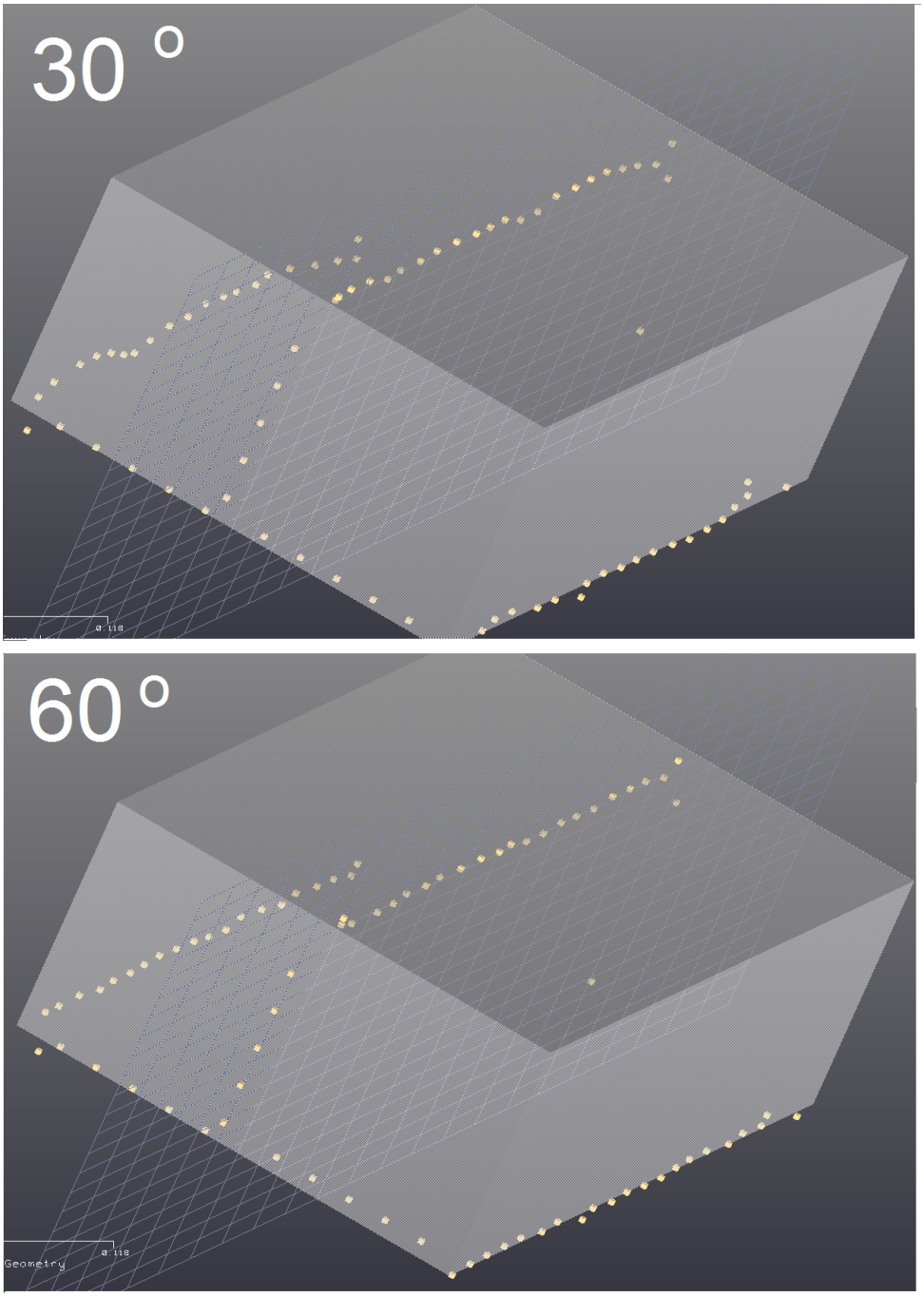

Figure 31: The animation of the velocity levels of the 79 measurement points. The phase increments are shown in the figure.

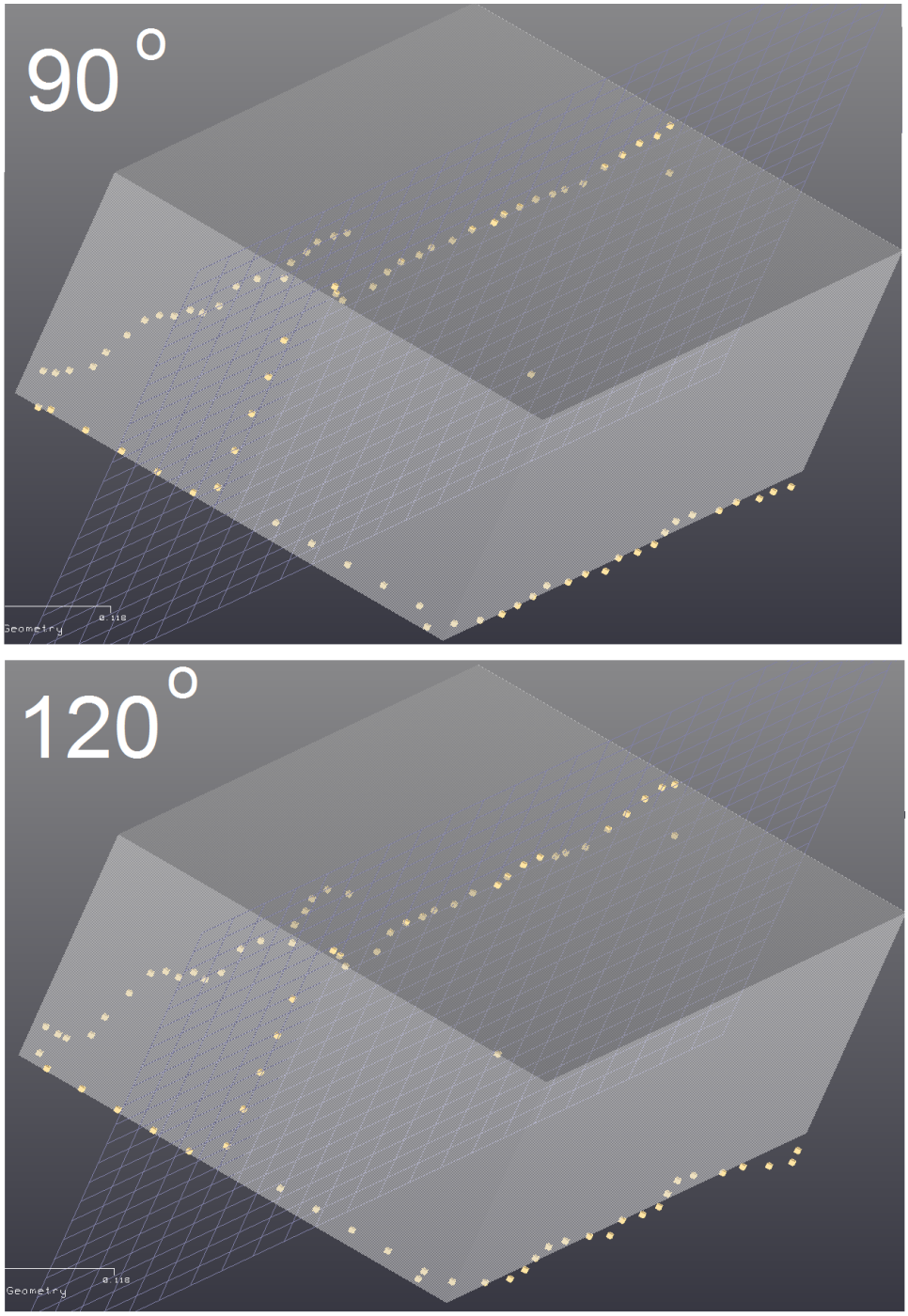

Figure 32: The animation of the velocity levels of the 79 measurement points. The phase increments are shown in the figure.

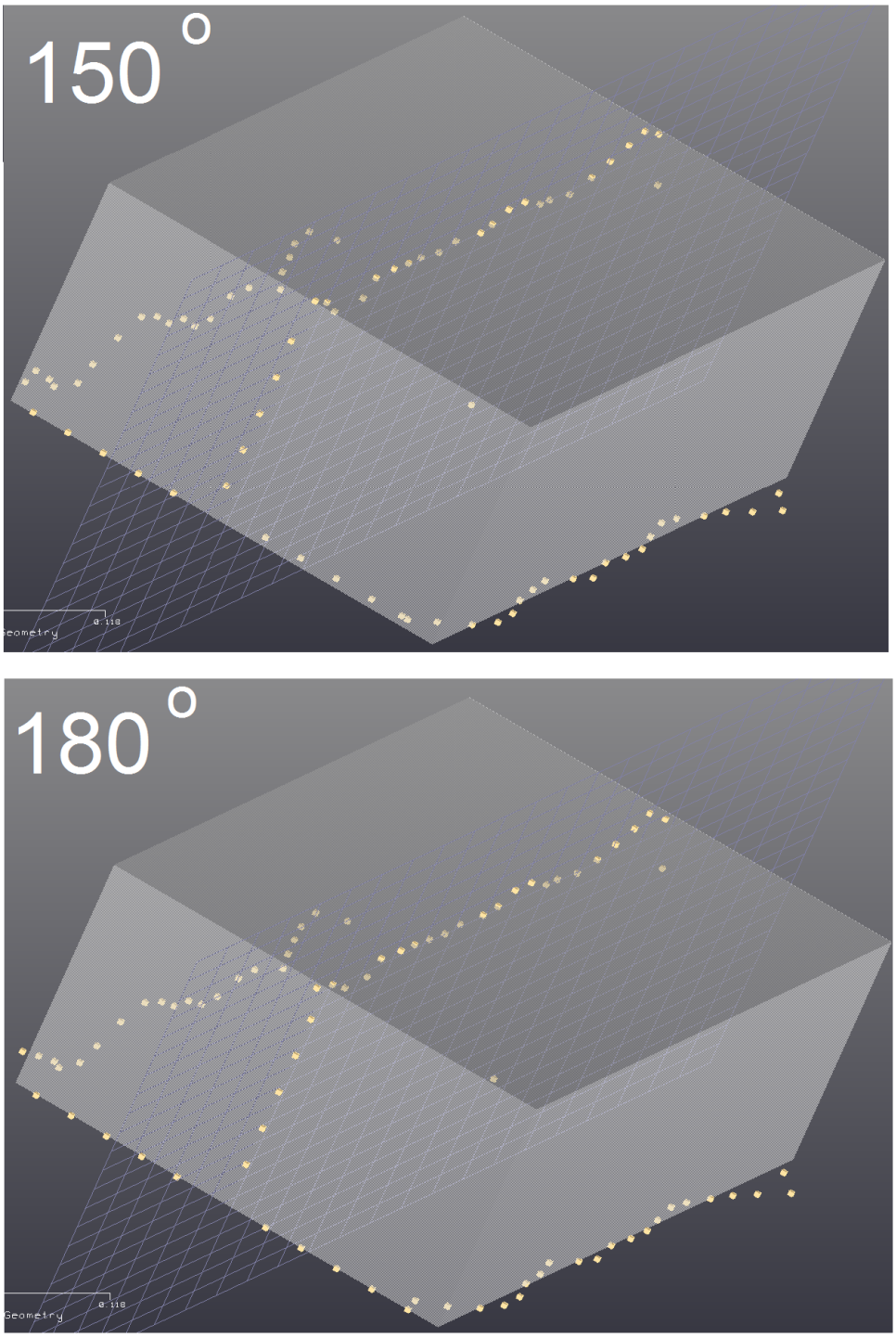

Figure 33: The animation of the velocity levels of the 79 measurement points. The phase increments are shown in the figure.

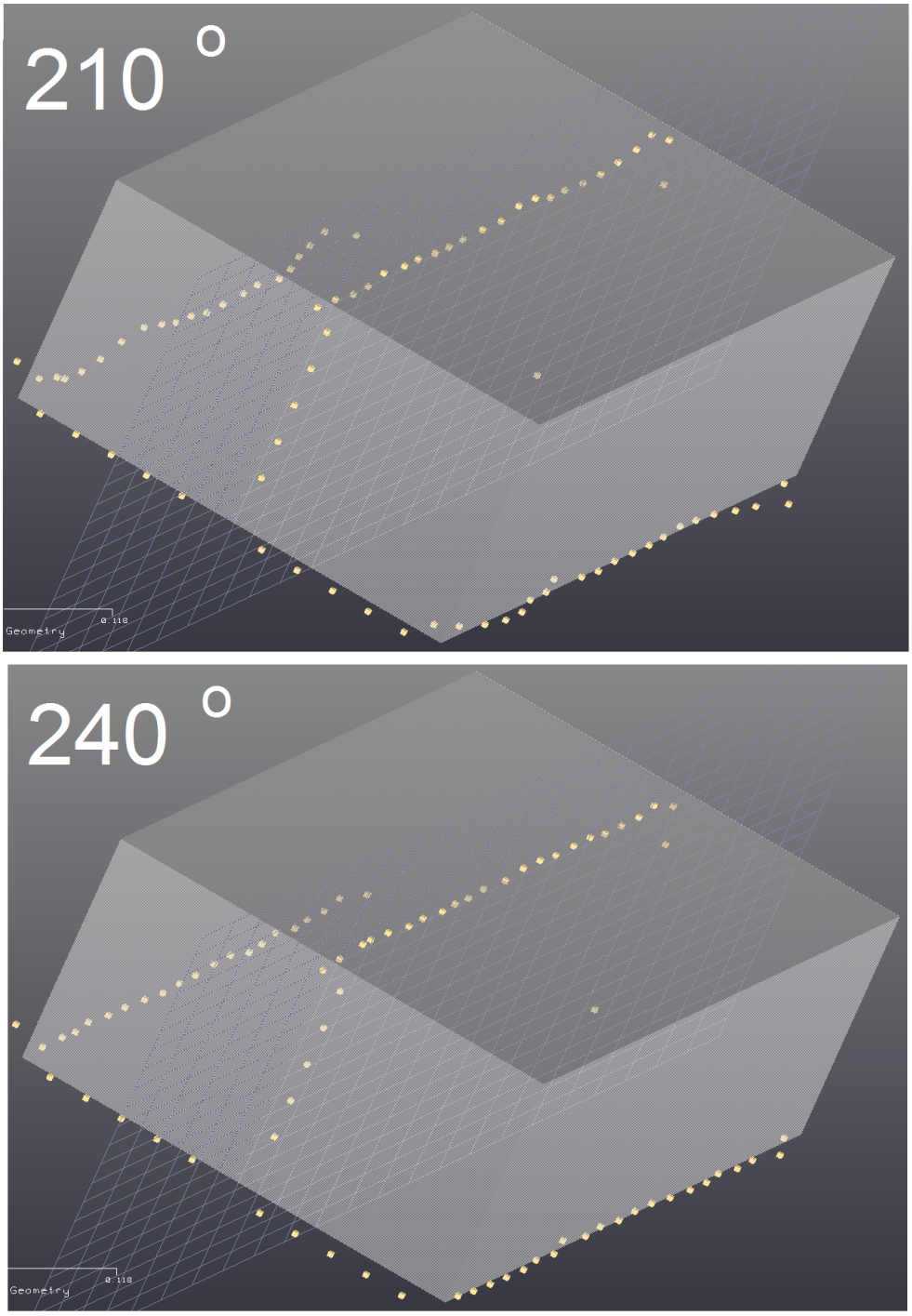

Figure 34: The animation of the velocity levels of the 79 measurement points. The phase increments are shown in the figure.

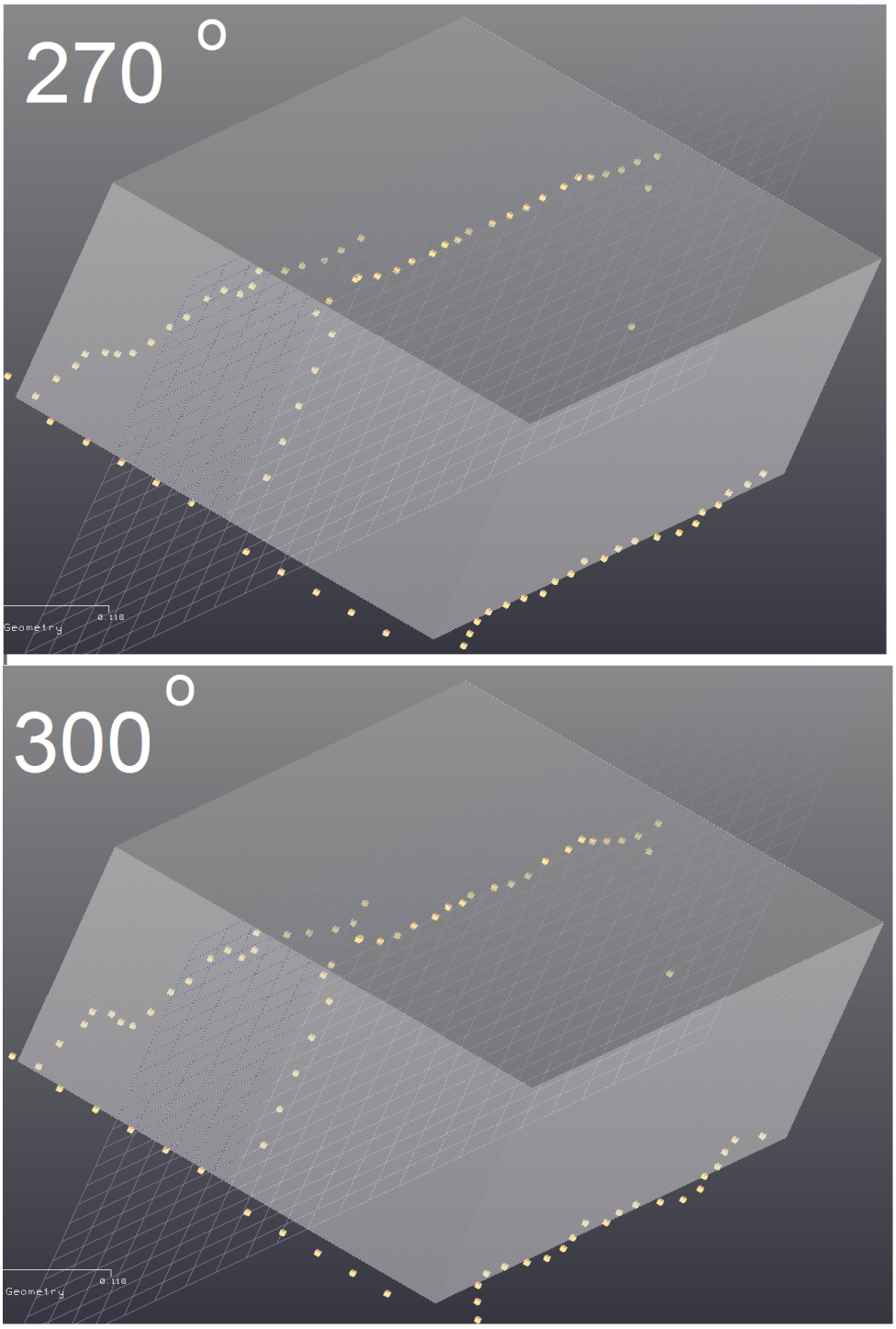

Figure 35: The animation of the velocity levels of the 79 measurement points. The phase increments are shown in the figure.

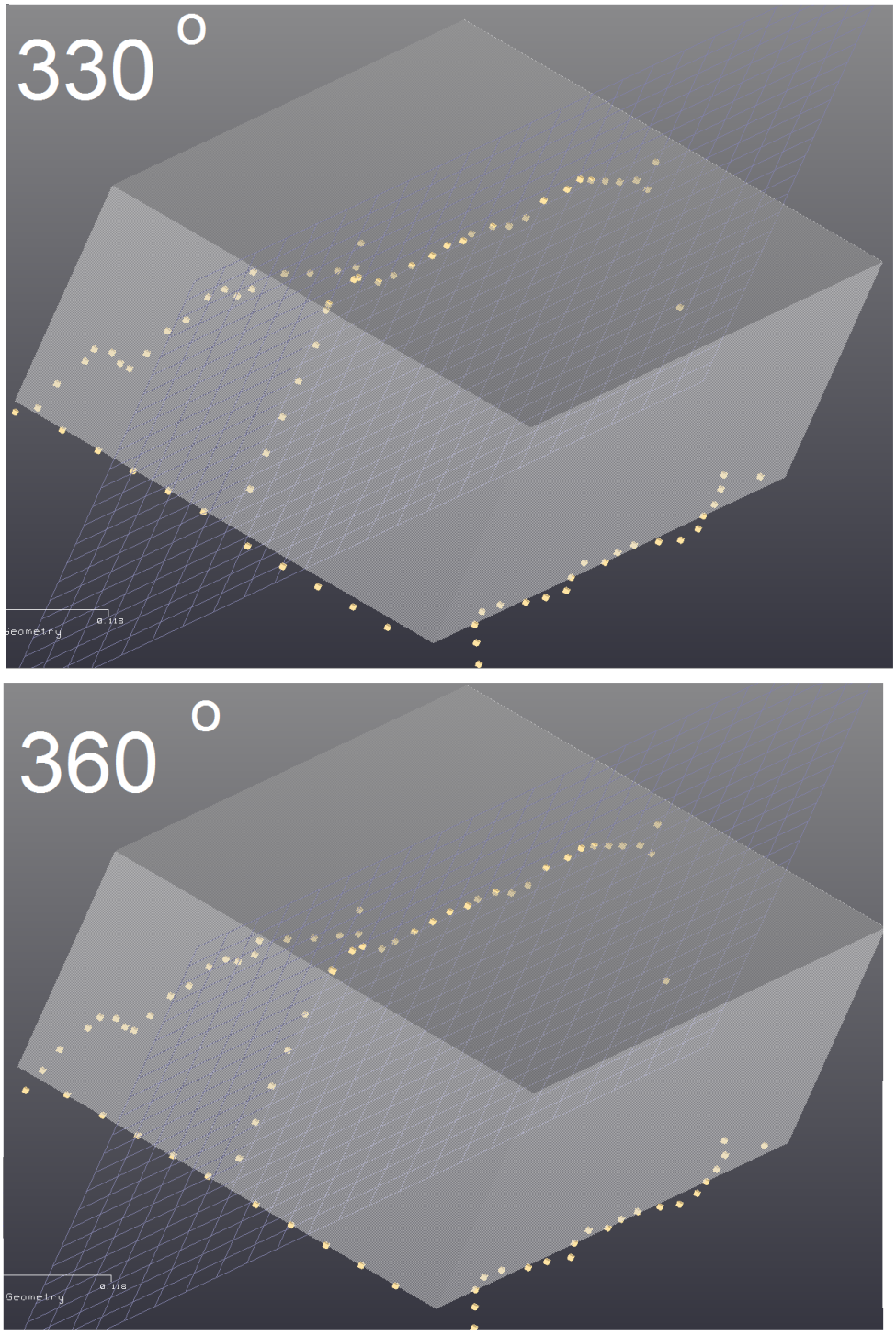

Figure 36: The animation of the velocity levels of the 79 measurement points. The phase increments are shown in the figure.

It is seen, most clearly, in the measurement points on the sides of the cylinder, that it is some kind of near field effect present on the edges of the cylinder. This is due to the free boundary conditions of the cylinder. Also, if looking closer at some points on the top and sides of the cylinder, it is possible to see that we have some

kind of wave motion of the particles, corresponding to the motion of a Rayleigh wave (described in section 2.7). If looking at the measurement points at the bottom of the cylinder, it is seen that this motion is much more plain, implying that the longitudinal wave is influencing this surface.

In figure 37, the wavelength of Rayleigh waves on the cylinder of nylon, is shown, following the calculations found in section 2.7.1. It implies that at a certain depth into the cylinder, in high enough frequencies, there will be little or no effect of Rayleigh waves, and here we assume that there are mostly longitudinal waves present (in depth of the cylinder).

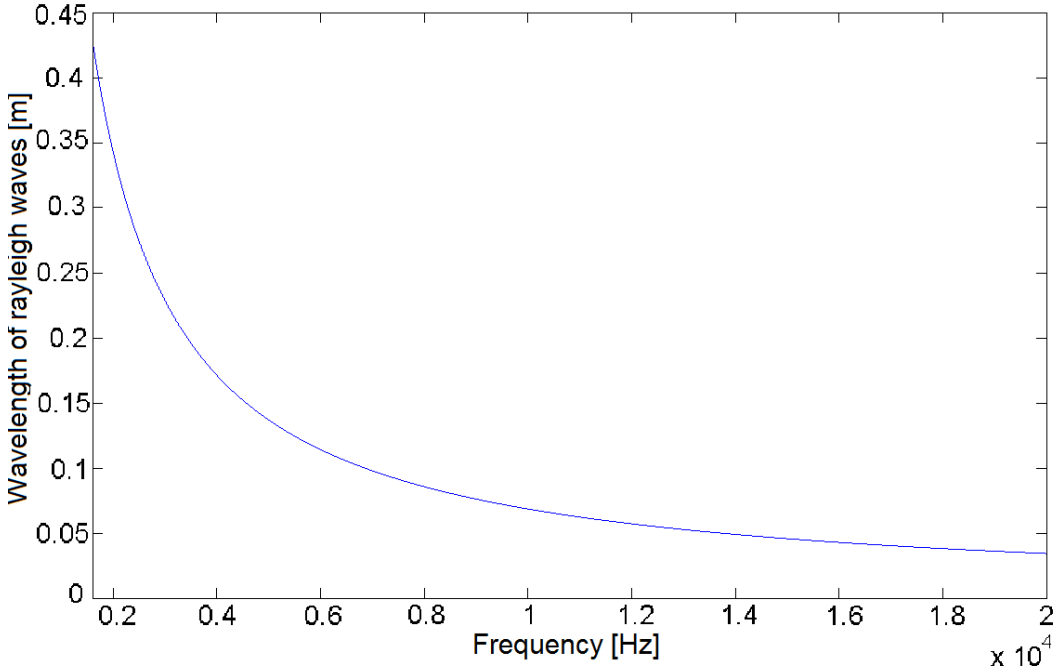

Figure 37: The wavelength of Rayleigh waves over frequency (nylon).

In figure 38, and 39, the velocity levels in the point on the mantle surface, near the bottom side (position 21), and just at the top of the bottom side (position 22) is compared. The 1st directional coordinate in this data stands for the measurement direction (relative to the coordinate system in figure 31). The 2nd directional coordinate in this system is the direction of the phase reference (acc2).

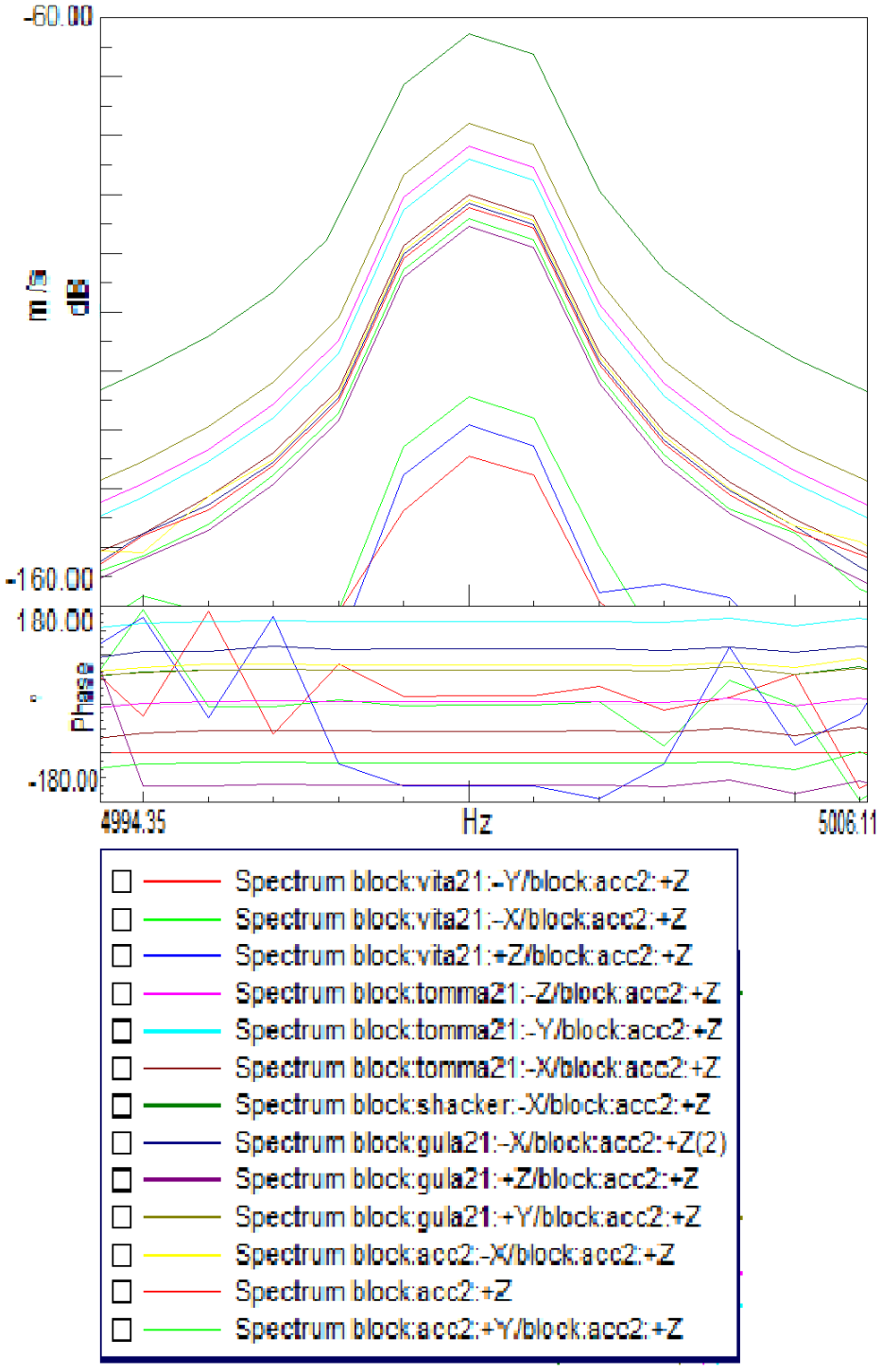

Figure 38: The velocity levels in the point on the top row of the mantle surface, closest to the bottom side (position 21).

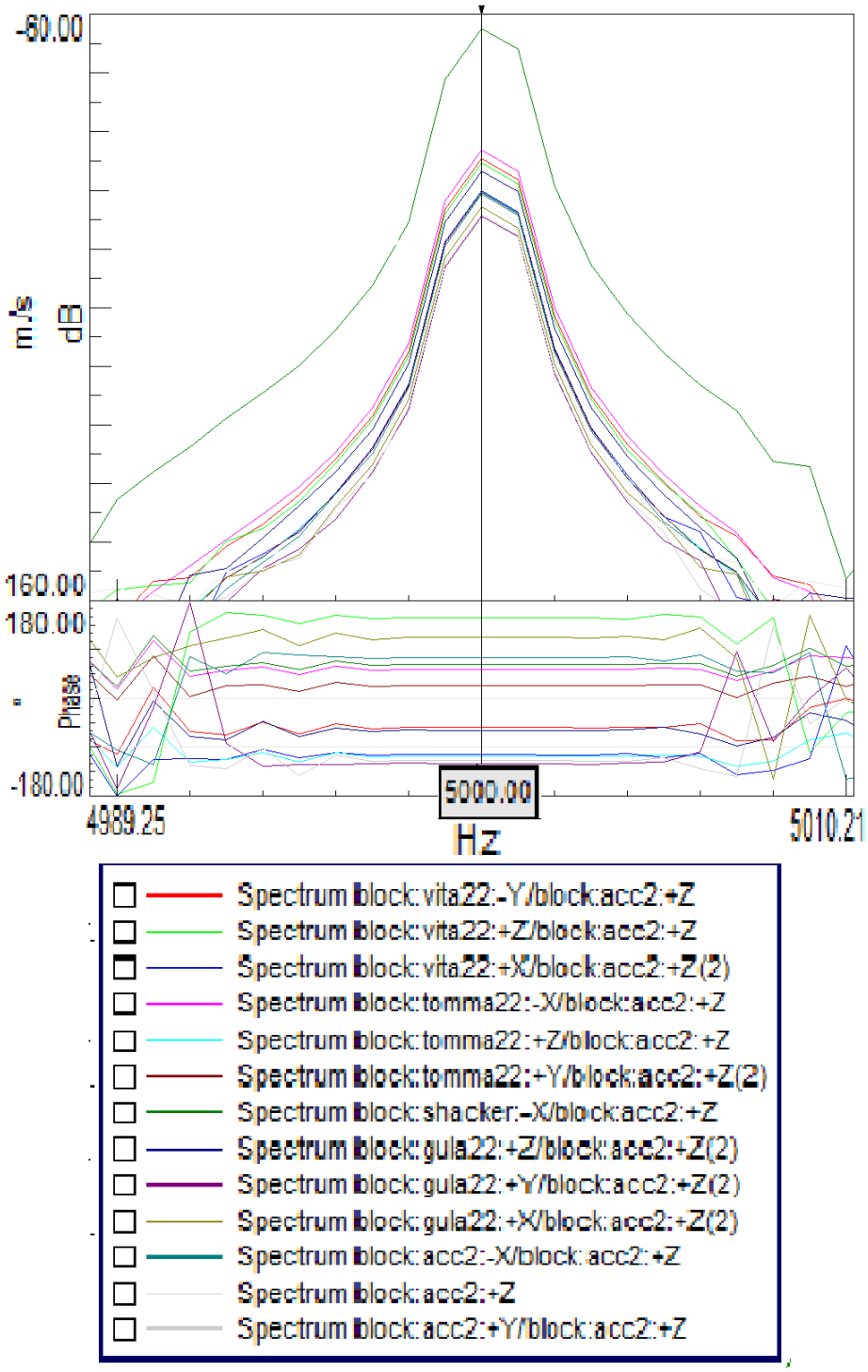

Figure 39: The velocity levels just at the top of the bottom side (position 22).

If looking at figures 38, and 39, it is seen that the majority of the velocities are comparable in level. The exception may be, that the velocity levels of the accelerometer on the mantle surface, "vita21", and the same accelerometer just below, "vita22", on the bottom surface, have a large difference in level. The level just below the

mantle surface, at the bottom surface, appears to be in the interval of 50 dB higher. Looking at the animation in .avi format, it is obvious that we do not have the same kind of retrograde motion at the bottom surface, as on the mantle surface. It is likely, we have a contribution from both longitudinal waves and Rayleigh waves at the bottom surface. This will make a problem for the modelling process, as it must be determined whether to use the velocity of a longitudinal wave or the velocity of a Rayleigh wave, on the respective surfaces. Although, it is assumed, in the model, that this velocity will be that of a Rayleigh wave. This is a fair estimation made for the model, as it is assumed that one wave type is present per sub-system. It is also a question, if the Rayleigh wave undergo some kind of transition, moving from the mantle surface to the bottom surface (as described in section 2.7.1 - 2.7.2).

4 Implementation

In this section, it is described how the velocity inside the cylinder is estimated, since we were unable to measure it (because the desired object did not arrive in time). An estimation of the lower limit of applicability of the SEA-model, is also described. Subsequently, the SEA-model is set up. This includes setting up the different subsystems, and finding the modal densities, internal loss factors, coupling loss factors, and input powers.

4.1 Theoretical estimation of the velocity in the cylinder

In order to be able to estimate the velocity in the interior of the cylinder, a plane wave model was used (since it was not possible to measure this velocity for our project). One can start by using the Euler-Bernoulli theory for beams, described in section 2.10. This presume that we view our cylinder as a beam-like structure, equivalent to a cylinder of long length. An assumption is made, that is based on a 1D theory, since we have a nice symmetry of our cylinder (excitation in the middle). This may not be entirely according to our real case, since we will likely have more of a spherical pressure wave field (diffuse field) at higher frequencies.

The setup of the measurements is given in figure 40, where the input force is taken from the measurements with the shaker.

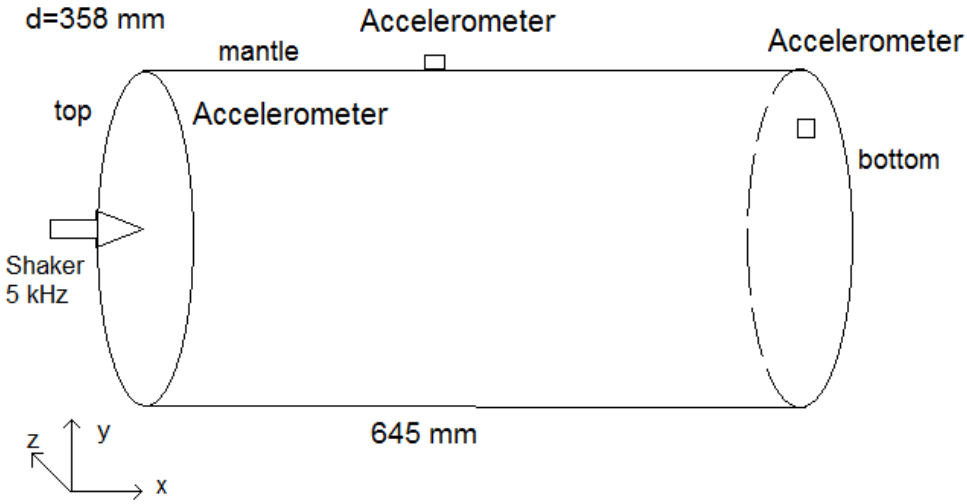

Figure 40: Measurements on the cylinder of nylon. The input force is taken from the measurements with the shaker.

In our case, with a free surface, the reflection factor, at the bottom surface, will be a real value of -1, for a 1D case.

The force, that is input on the cylinder, is:

$F = 1.06$ N

And using eq. (6) of section 2.10, it is possible to calculate the displacement in the

cylinder using the measurement data. Deriving this, we have the absolute value of the velocity, which will be:

$V_{cal} = 5.3185 \cdot 10^{-6}$ m/s

The calulated value will then be an estimated velocity inside the cylinder, of a longitudinal wave moving in the cylinder, which explains why this value is lower than the measured value, at the top side (the excited side) of the cylinder. Naturally, the wave will "die" out, while travelling through the material, mainly due to damping. This value is later used to compare the velocities of the measurements and velocities from the SEA-model.

Note: this value may not be a complete picture of the reality, but it could be a good approximation. It is also somewhat uncertain, since it is based on measurement data of a single measurement point.

4.2 Setting up the SEA-model

Now that all the parameters required for the SEA-model are found, it is possible to build it. The following in-data are required for the basic analysis:

- Young's modulus
- Density
- Shear modulus
- Poisson's number

The most of this data were found in the manufacturer's data sheet, in [25], for our cylinder of nylon (PA6TECAST). The density was found to be: $\rho = 1150$ kg/m^3, the young's modulus was found to be: $E = 1700 \cdot 10^6$ N/m^2, and the Poisson's ratio was estimated from other values for nylon, to be: $\nu = 0.39$. The SEA sub-systems are chosen according to figure 41.

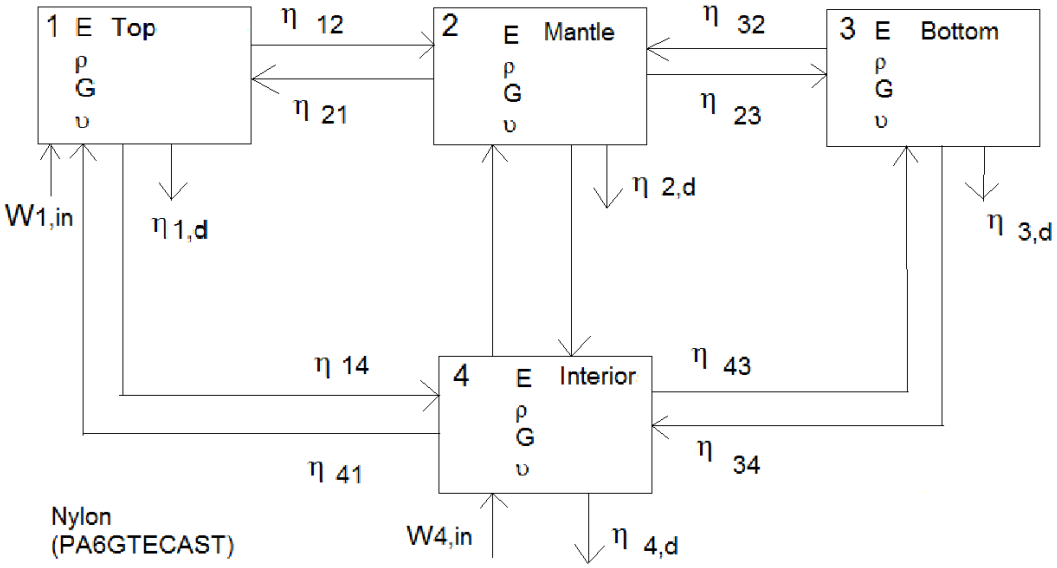

Figure 41: The SEA sub-systems, for our model of nylon.

It is indicated (according to section 2.7 - 2.7.1), that the surface waves (Rayleigh waves) will be present in sub-systems 1-3. It will also have a minor effect on the interior/volume (neglected in this report). It is assumed that it is only longitudinal waves present in sub-system 4. The Rayleigh waves in sub-system 2, will have a different velocity from the Rayleigh waves on the smaller surfaces, due to the curving of the cylinder (see section 2.6.1).

It is also assumed that there are **weak coupling** between the sub-systems, meaning that there are large internal losses in comparison to the energy transferred between the sub-systems.

The model calculations were divided into two theoretical cases.

1. In the 1st case, all the input power goes into sub-system 4.
2. In the 2nd case, the input power into sub-systems 1 and 4, are given from the distribution described below.

It is possible to implement the integral expressions of (3), (4), and (7), from section 2.8, into MATLAB, and solve for a specific value of Poisson's ratio, ν. This gives an approximation of the distribution of energy between wave types, for longitudinal, shear, and Rayleigh waves, for a point excitation on a half-infinite solid. The results from these calculations are found in table 3, for two different values of Poisson's ratio, $\nu = 0.25$, $\nu = 0.39$, of which the latter gives the data for our cylinder of nylon.

	Longitudinal wave (%)	Shear wave (%)	Rayleigh wave (%)
For $\nu = 0.25$	6.88	25.75	67.36
For $\nu = 0.39$	3.84	34.85	61.31

Table 3: The distribution of energy between wave types, for longitudinal, shear, and Rayleigh waves (for $\nu = 0.25$, and $\nu = 0.39$).

The input power in the model relative to what we had in the measurements, are neglected, and instead we use only a unit power input (P=1 W), into the model. This doesn't matter, because we only compare the relative differences between the velocities.

4.3 Lower limit of applicability

It is possible to use the formula for the lower limit of applicability for the SEA analysis (see section 2.8.1), for the case of a nylon cylinder, for both longitudinal waves and Rayleigh waves. In table 4, the results from these calculations, are given, for longitudinal waves.

Freq.	1k	1.25k	1.6k	2k	2.5k	3.15k	4k	5k	6.3k	8k
M	0.78	1.02	1.40	1.90	1.87	4.38	7.80	12.01	16.91	24.08

Table 4: The lower limit of applicability for the SEA-analysis, for longitudinal waves.

This result shows that the SEA-analysis could be valid for frequencies higher than between 1 kHz, and 1.25 kHz, for longitudinal waves. The same result, but for Rayleigh waves, are given in table 5.

Freq.	250	315	400	500	630	800	1k	1.25k	1.6k	2k
M	0.74	0.96	1.24	1.62	2.18	3.02	4.15	5.80	8.55	12.36

Table 5: The lower limit of applicability for the SEA-analysis, for Rayleigh waves.

This indicates, that the results could be better for Rayleigh waves, at lower frequencies.

4.4 Modal density

The modal densities in this section, for a steel block, as a reference, and for the cylinder of nylon, are calculated according to formula (3) of section 2.8.4.

The modal density for a block of steel, of dimensions 1000x1000x500 mm, is shown

in figure 42. The block of steel has a density of: $\rho = 7800$ kg/m^3, a Poisson's ration of: $\nu = 0.3125$, and a young's modulus of: $E = 2.1 \cdot 10^{11}$ Pa.

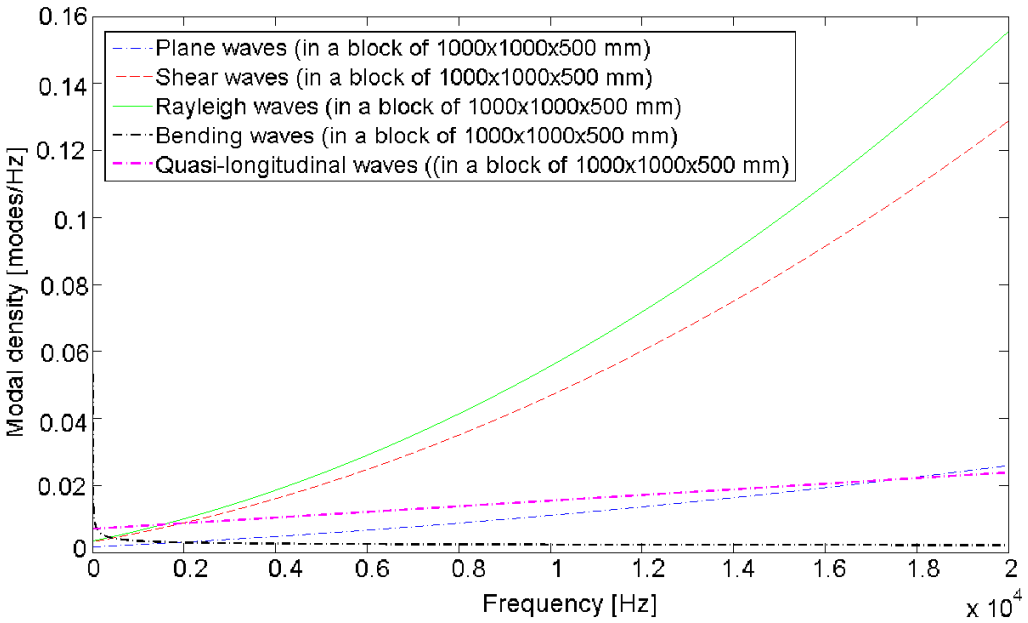

Figure 42: The modal densities for a block of steel of dimensions 1000x1000x500 mm, for longitudinal- shear, Rayleigh, and quasi-longitudinal waves. The modal density of bending waves for a block of steel of of dimensions 1000x1000x500 mm is also shown.

The modal density for a block of steel, of dimensions 1000x1000x500 mm, is shown in figure 43, in 3rd octave bands.

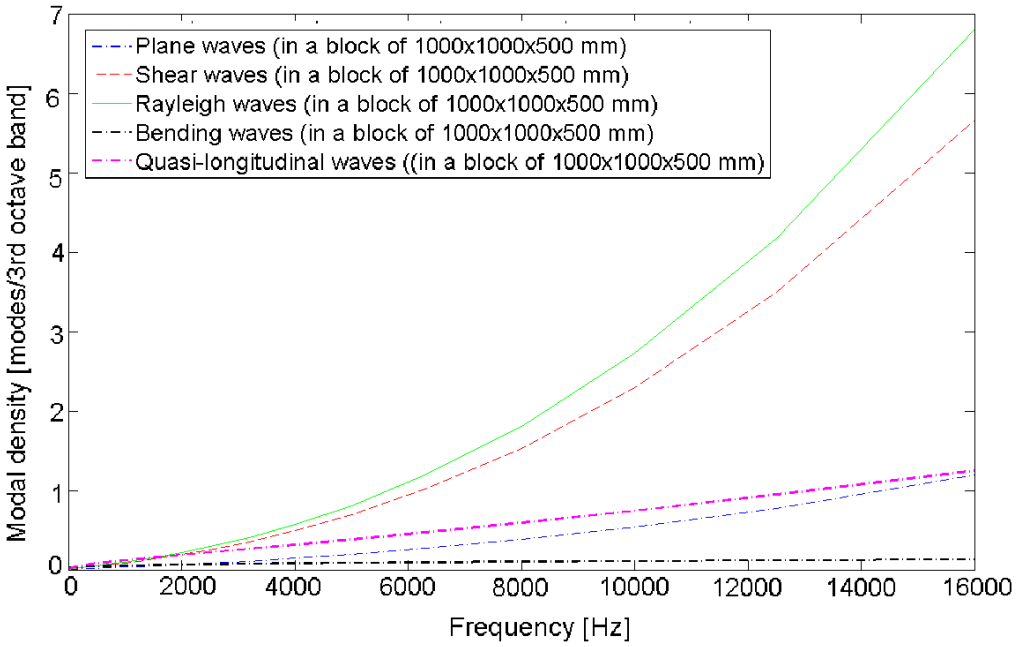

Figure 43: The modal densities for a block of steel of dimensions 1000x1000x500 mm, for longitudinal- shear, Rayleigh, and quasi-longitudinal waves, in 3rd octave bands. The modal density of bending waves for a block of steel of dimensions 1000x1000x500 mm is also shown.

The velocity of the Rayleigh waves on the curved surface, used for calculating the modal density on the curved surface (mantle) of the cylinder, is calculated from the derivations found in section 2.7.1. In figure 44, the velocity of a Rayleigh wave is given, over frequency, for a curved surface having radius of curving in α and β-direction, $\rho_\alpha = 0.179$ m, $\rho_\beta = 0.179$ m. This curved surface is made of nylon, having a density of: $\rho = 1150$ kg/m^3, a Poisson's ration of: $\nu = 0.39$, and a young's modulus of: $E = 1.7 \cdot 10^9$ Pa.

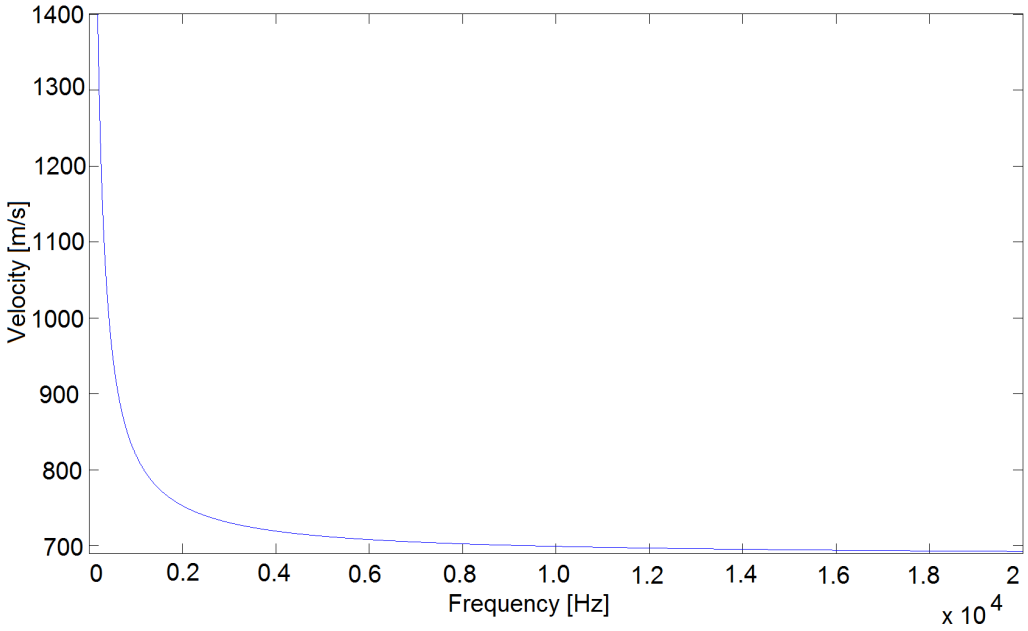

Figure 44: The Rayleigh wave velocity on a curved surface having radius of curving in respective direction, $\rho_\alpha = 0.179m, \rho_\beta = 0.179m$ (nylon).

Note: The velocity of the Rayleigh waves on a curved surface, is based on a "smooth" curving, which is approximated to be close to the case of Rayleigh waves, moving in any direction, over the surface of a cylinder.

The modal density for a cylinder of nylon (PA6GTECAST), of dimensions 645x358 mm, is shown in figure 45, in 3rd octave bands. The cylinder of nylon has a density of: $\rho = 1150$ kg/m^3, a Poisson's ration of: $\nu = 0.39$, and a young's modulus of: $E = 1.7 \cdot 10^9$ Pa.

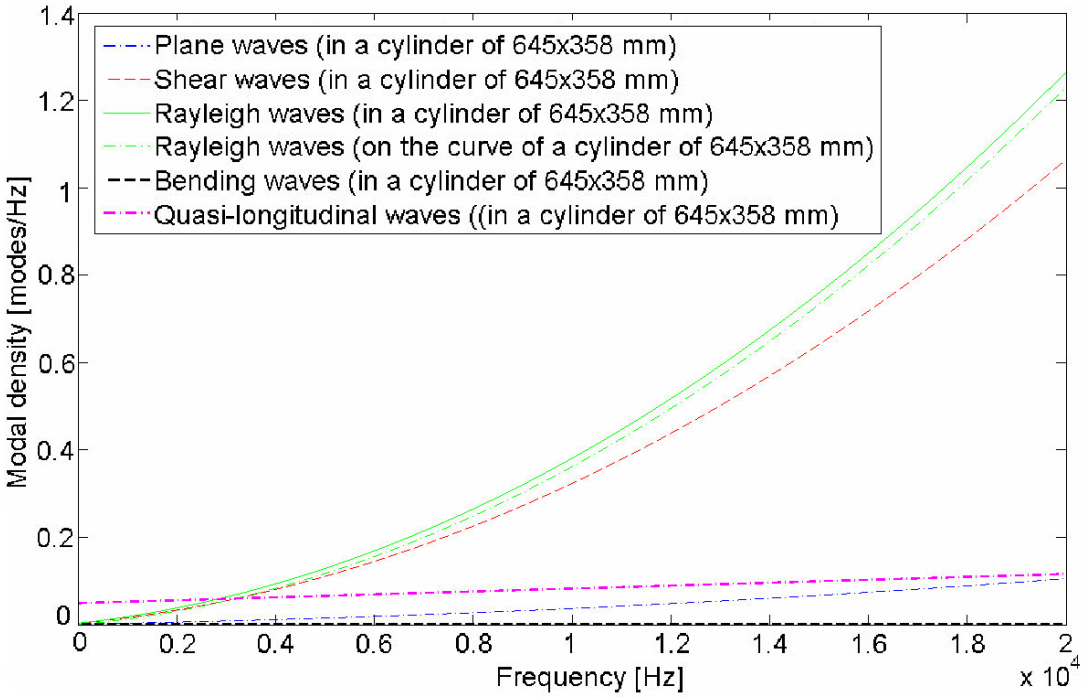

Figure 45: The modal densities for a cylinder of nylon of dimensions 645x358 mm, for longitudinal- shear, Rayleigh, and quasi-longitudinal waves, in 3rd octave bands. The modal density of bending waves for a cylinder of nylon of of dimensions 645x358 mm is also shown.

4.5 Coupling loss factors

The coupling loss factors for the Rayleigh waves, moving from the mantle surface of the cylinder, to the top/bottom surface, and the reverse, needs to be estimated. Somewhat, we assume that the Rayleigh wave moving on the surface of the medium, toward the corners, can be seen as a 2D type junction, which is why formula (1) of section 2.8.7 is used. The results for the power transmission coefficient, calculated from the derivations in section 2.6.2, and using formula (8) of the same section, is:

$T_{power} = \tau_{21} = \tau_{12} = \tau_{23} = \tau_{32} = 0.9405$

The value of the amplitude transmission coefficient, that was found from this method, was $T = 0.7561$. This seems to be quite good in correlation with the results for the $\approx 90^o$ wedge that was found in [22].

The results are presented in figure 46, for the coupling between the mantle and bottom/top.

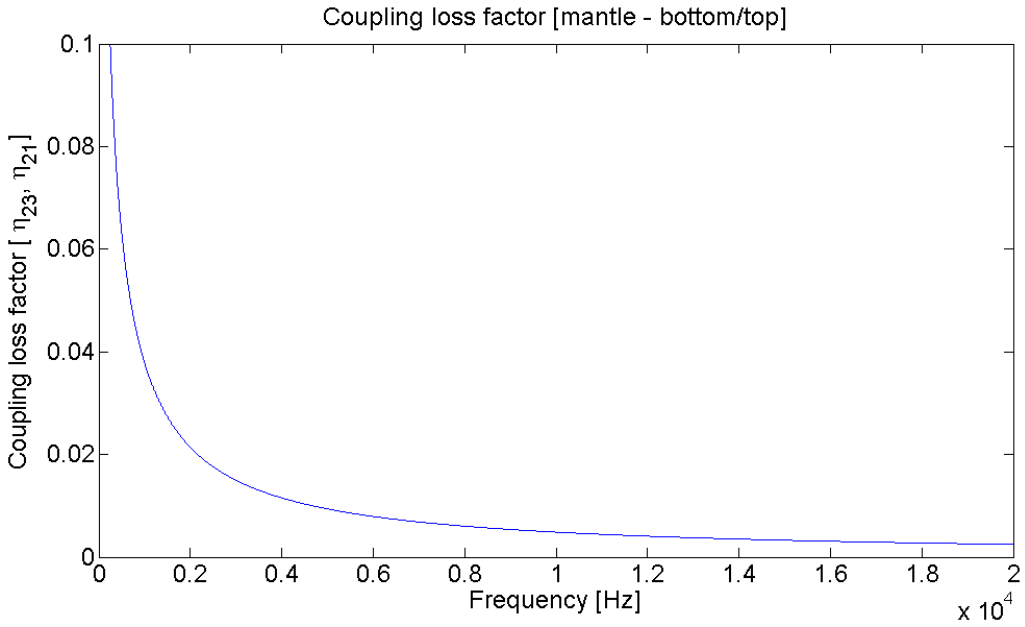

Figure 46: The coupling loss factors between the mantle and bottom/top.

The coupling loss factors from a longitudinal wave, in the interior of the cylinder, to Rayleigh waves, on the surfaces, is calculated using formula (2) of section 2.8.7. It is given in figure 47. The reverse, coupling loss factors from the Rayleigh waves to longitudinal waves, are calculated using the reciprocity relation (7) of section 2.8.8. All these values are estimated to be close to neglectable, in accordance to the theory in 2.7.2 (where it is fully neglected). This was done by choosing the value of the power transmission coefficients, τ_{41}, τ_{42}, τ_{43}, τ_{14}, τ_{24}, τ_{34}, to be 0.01^2. If a non-neglectable transmission is assumed, the transmission between the longitudinal waves and Rayleigh waves would take place at the corners, according to [22].

Note: if one have a corrugated type of surface (non-plane), or up-and down-steps, one will although have transmission of energy between wave types, also at the surfaces, and this is described in [31], [32], and [33]. This means that a longitudinal wave will be converted to a Rayleigh wave on an uneven surface, and also the reverse.

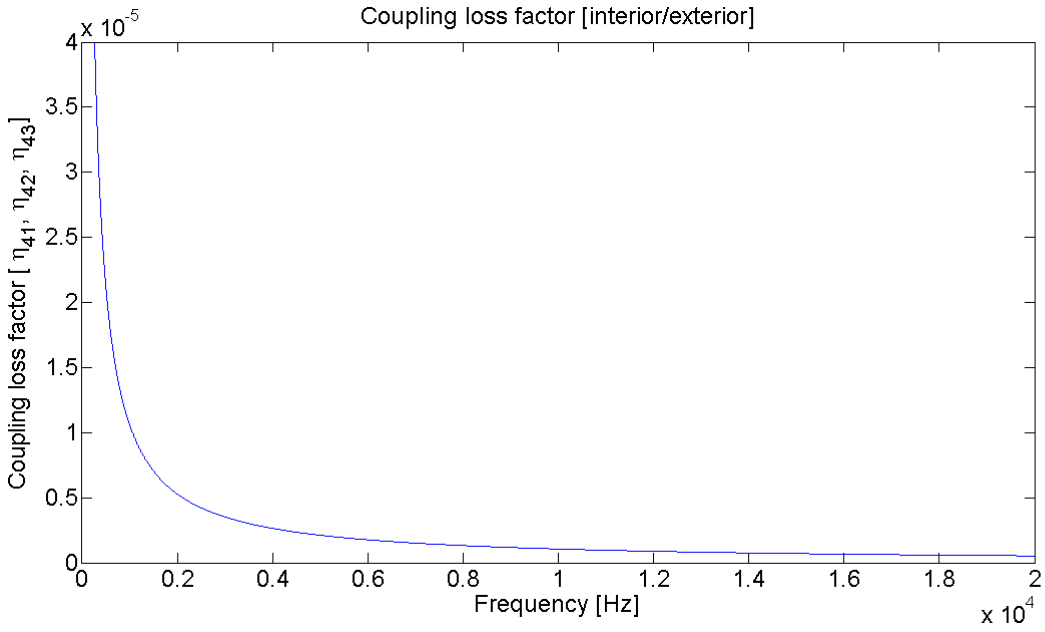

Figure 47: The coupling loss factors between the interior and exterior of the cylinder.

5 Results

After calculations in MATLAB, the velocities were found from the modal energy. These were calculated using the energy balance, as described in section 2.8.10. Note: for cases, differing from our, where for example the object under consideration is very large, or a medium with very short wavelengths of a Rayleigh wave, the energy balance is likely have to be compensated, for the part of the mass actually concerning the movement of Rayleigh waves. There are two modeling cases described in the results, and these are described in detail in section 4.2. The velocity levels, for case 1, are given in figure 48.

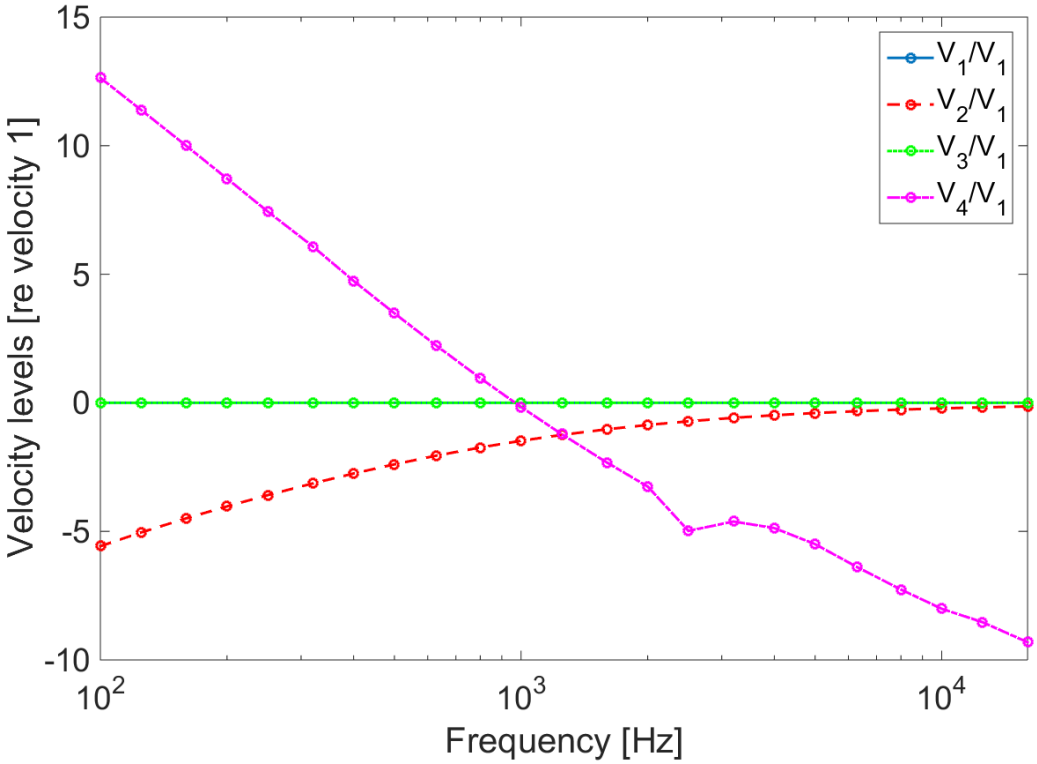

Figure 48: The velocity levels in 3rd octave bands (in a dB scale). For case 1.

The velocity in the 4th sub-system (relative to sub-system 1), the interior, seems to be decreasing, for this case, and crosses the value of the velocities at the top and bottom side, at around 1 kHz. There is also a small dip between 2 and 3 kHz, which could likely be an error in the modelling process. The differences between the top (sub-system 1) and bottom side (sub-system 3), are neglectable. The velocity in the 2nd sub-system, which is the mantle, is slightly increasing over frequency. This result, indicates, that we may have an over-estimation of the velocity inside the cylinder, at lower frequencies. This could make sense, as it is assumed, in case 1, that the full power input goes into the longitudinal wave in the interior.

The results, for case 2, is given in figure 49, having a power input of largest magnitude into the 1st sub-system, and a small part into the 4th sub-system, as described in section 4.2.

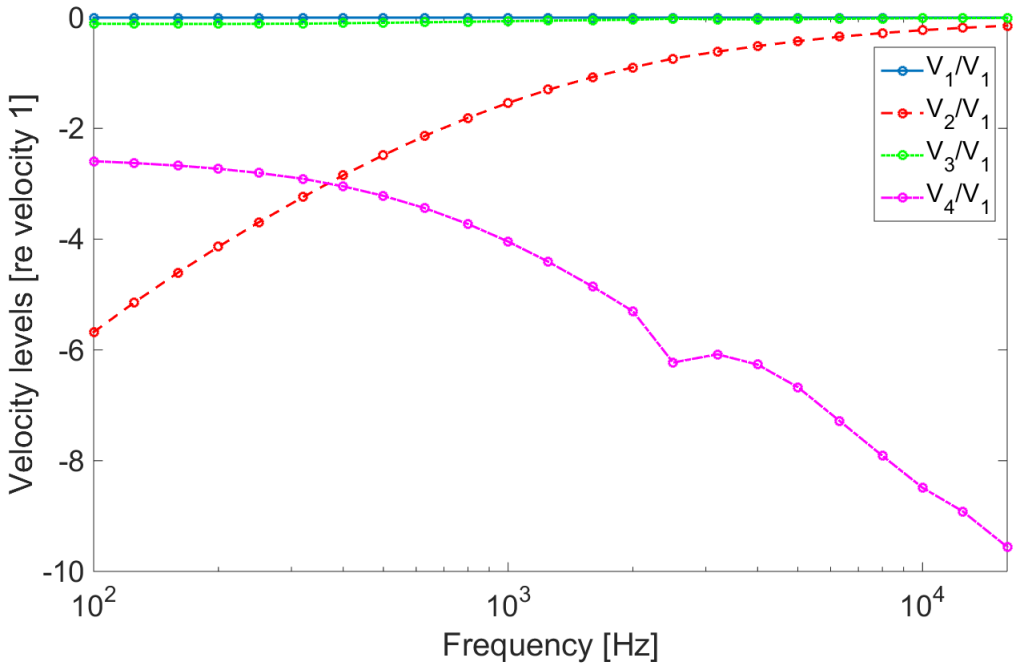

Figure 49: The velocity levels in 3rd octave bands (in a dB scale). For case 2.

It is seen, that the velocity of sub-system 4 (relative to sub-system 1), the interior, seems to be decreasing, from a lower starting value than for case 1. This is likely due to the fact that we have only a small part of the energy going into the longitudinal wave, in sub-system 4 (as described in section 4.2), and most energy going into the Rayleigh wave in sub-system 1. The relative velocity in sub-system 2, the mantle, seems to be slightly increasing over frequency, and this velocity is quite similar to the velocity in the 1st case. The relative velocity in the 3rd sub-system is increasing, and gets closer to the velocity in sub-system 1. This 2nd case, with the given distribution of power, gives a result that mostly seems to affect the relative velocity in the 4th sub-system.

5.1 Comparison of the model and mesurements

In order to have a picture of the differences between the results from the model, and from the measurements, dB values are given as the difference between the measured values and the model values. The results from the comparison between measured values (from section 3.3), theoretically estimated value for sub-system 4 (from section 4.1), and model values, from the above section, are found in table 6, for 5 kHz.

	Velocity 1	Velocity 2	Velocity 3	Velocity 4
Case 1 (power input into sub-system 4)	1.0000	0.9552	1.0000	0.5311
Case 2 (power input from calculations)	1.0000	0.9552	0.9968	0.4861
Measured (rel. velocity 1)	1.0000	1.1150	1.6430	0.2204
Case 1 (difference in dB between the measured values and model)	0 dB	-1.3 dB	-4.3 dB	7.6 dB
Case 2 (difference in dB between the measured values and model)	0 dB	-1.3 dB	-4.3 dB	6.9 dB

Table 6: Comparison of values from the 4 different cases, and the measurements/estimations, at 5 kHz. Velocity 4 in the row for measured values is an estimated value based on a plane wave model (from section 4.1). All these values are relative to these in sub-system 1.

The results, shown in table 6, indicates that case 1 may be overestimating the influence of the longitudinal wave (sub-system 4). This is strengthened by the fact that the transmission from longitudinal waves to Rayleigh waves, are assumed to be neglectable. The 2nd case, seems to give better overall results than the 1st case, introducing the distribution of energies found in section 4.2. Comparing the results from the measurements, to those from the model, indicates that we may have an effect from the longitudinal wave, on the bottom side, which could be the reason why this value is higher, compared to the model values. This is also seen when looking at the animations of the cylinder. The 4th velocity in the measurements row, are actually not fully measured, but based on a plane wave model, incorporating measurement data (see section 4.1).

Note: in order to have a correct measurement of the velocity inside the cylinder, one would have to use a transducer inside the cylinder, retaining the original boundary conditions. One possible way of doing this would be to place a hole, fitting the transducer, inside the cylinder (easiest to achieve by making a cross-section of the cylinder. This could look something like shown in figure 50.

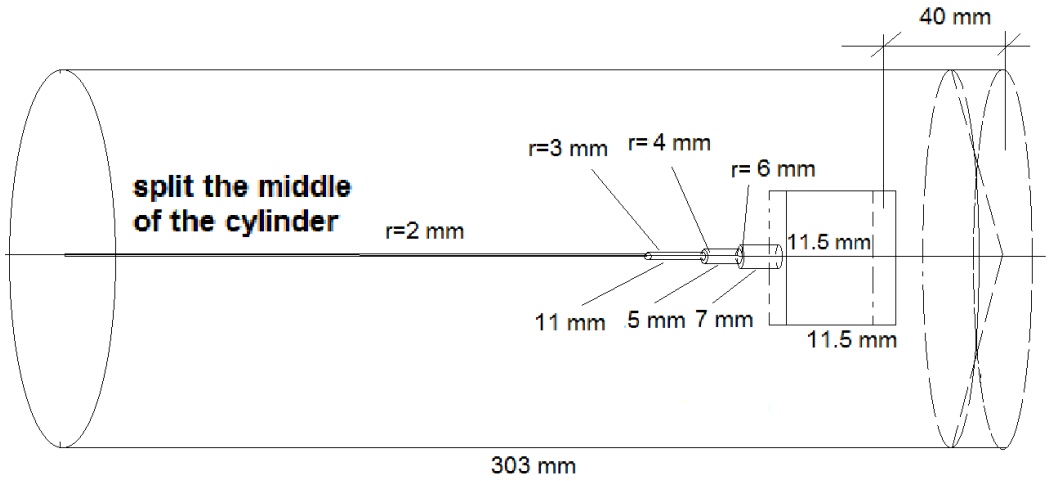

Figure 50: The sketch of the proposed technique for measuring the velocity inside the cylinder.

6 Discussion

In this section, the implementation of the model, and the measurements executed on the cylinder of nylon, are discussed. Also, the estimation of the velocity in the 4th sub-system is discussed. Differences between the measurements/estimations and the model are discussed and evaluated. Also, it is looked upon what possibly needs to be corrected in order to have a proper "input run" model, where it is possible to use different materials and geometries. There are, to judge from the results presented in this report, two main factors affecting the end result, and this is the distribution of excitation energy between wave types, and the transmission of energy between sub-systems. The transmission of energy between longitudinal waves and Rayleigh waves, are actually neglectable in the theory being used (as described in section 4.5). The measurement data and model data have some large deviations. One reason for the high values of the measurement at the bottom side (sub-system 3) could be that the velocity is affected by the longitudinal wave, moving through the cylinder (as mentioned in section 3.3), from the excitation point. In the SEA-model, the velocity on this face is estimated for the Rayleigh wave only. Also, the estimated data, for the 4th sub-system, may not to well reflect the reality, since it is based on a solely plane wave model (as described in section 4.1). Likely, our "real" world case would be more of a spherical pressure wave field, at least in the higher frequencies, where we likely have a diffuse field of waves. Another doubt, is that the Rayleigh wave could be affected by the depth of the cylinder. The wavelength of a Rayleigh wave, is, as shown in section 3.3, comparable to (or shorter than) the dimensions of the cylinder, for higher frequencies. This may have to be compensated for when doing the calculations of the velocities, as described in section 5. Also, our measurements were only done in 1 specific frequency, which can be compared to the calculated velocity in that frequency band. Maybe, the most important part of the doubts are the calculations of the transmission coefficients. These are done in a most theoretical way, giving the result described in section 4.5. The measurements of the reverberation times, and the calculated loss factors, are hopefully somewhat correct. Also, as explained, the input power in the SEA-model is a big doubt, as we may have a distribution of the energy between the longitudinal waves and the Rayleigh waves, as described in section 4.2. Overall, the correlation of model data, and measured/estimated values, were a little better for case 2, introducing the calculated distribution of energy (as seen in figure 50).

7 Conclusions

In this report, the investigation concerns the relationship between the surface of a solid of nylon, and the interior of the cylinder, regarding wave motion. An established SEA-model, using MATLAB, and theoretical parts for establishing energy balance and coupling loss factors, have shown that it is at least theoretically possible, to implement the theory of SEA for a three dimensional object. There are still many large doubts when it comes to theoretical parts, and one of these are theory that were found in order to calculate the transmission coefficients for the Rayleigh wave moving over a wedge. A model was used, as described in section 4.5, that assumes neglectable transmission from longitudinal waves to Rayleigh waves. Other research in this area, however, have shown that it is possible that transmission between longitudinal waves and Rayleigh waves will occur, both at the corners, as described in [27], and also if the surfaces have discontinuities such as cracks and up-and down steps, as described in [31], [32], and [33]. This is a topic that is highly recommended for future work in this area. Another of these topics are measurements of the velocities in the interior parts of the cylinder (as proposed in section 5.1). This is, in this work, estimated by using a simple plane wave model, based on the measurement data, that could be highly inaccurate, since it does not reflect the kind of wave field, we would likely have at 5 kHz, which would be more of a spherical pressure wave field. This would be a field of work that is highly recommended for the future of similar projects.

8 Future work

Another interesting aspect, is in what frequency range this model could be valid. It is shown, in the estimation of the lower limit of applicability for the SEA-model, as given in section 4.3, that it is possible that this model is valid for somewhere between 1 kHz and 1.25 kHz, and above. But this is an estimation, and it is possibly necessary to compare the model with measurements in a broader frequency interval, to be able to tell. Also, the model and the measurements do not show the same trend, as seen in table 6, so it is necessary to make measurements in a broader frequency interval, also for this purpose. This means that it is still unclear whether this model gives a correct picture of reality or not, since it was not possible to execute the measurements that were required for a full validation. It would be of interest to make the measurements with "broadband noise", and also place a transducer inside the cylinder, for this measurement, as explained in section 5.1.

9 References

[1] Choudhury, D. [nptelhrd]. (2013). *Mod-03 Lec-15 L15-3 Dimensional Wave Propagation, Waves in half-infinite medium, Rayleigh Wave* [Video]. Avaliable: https://www.youtube.com/watch?v=J0VG0kbBSIM

[2] Telford, W.M.; Geldart, L.P.; Sheriff, R.E. (1990). *Applied Geophysics (2nd Edition).* Cambridge: Cambridge University Press

[3] Kutruff, H. (2007). *Acoustics - An Introduction.* Taylor & Francis. London and New York: Taylor & Francis Group

[4] W. Kropp. (2003) *Technical Acoustics 1 - lecture 9.* Gothenburg: Chalmers University of Technology - Department of Applied Acoustics

[5] D. Norgren; X. Wang. (2012) *Technical Acoustics 2 - Report: U-shaped structure vibration analyze part 1.* Gothenburg: Chalmers University of Technology - Department of Applied Acoustics (Undergraduate report)

[6] J. Plunt. (1998) *Statistical Energy Analysis (SEA) - Theory and Applications.* Gothenburg: Ingemansson Technology AB

[7] Lyon. R. H; DeJong R. G. (1995) *Theory and Application of Statistical Energy Analysis. 2nd Edition.* Butterworth-Heinemann

[8] Cremer. L.; Heckl. M. (1996) *Körpershall. 2nd Edition.* Springer Verlag

[9] Nashif A D, Jones D I G, Henderson J P (1985): *Vibration damping.* John Wiley

[10] Fahy F, J: Statistical Energy Analysis, (1982) *Noise and Vibration* (ed. White, Walker), Chapter 7, Ellis Horwood Publ

[11] T. Koizumi *, N. Tsujiuchi *, H. Tanaka *, M. Okubo **, M. Shinomiya **. *PREDICTION OF THE VIBRATION IN BUILDINGS USING STATISTICAL ENERGY ANALYSIS.** Department of Mechanical Engineering, Doshisha University, Kyotanabe, Kyoto 610-0321, JAPAN. ** YANMAR DIESEL ENGINE CO., LTD. 1600-4, Umegahara, Maihara, Sakata, Shiga 521-8511, JAPAN.

[12] D. M. Riffe. (2013). *Lecture 6 - Traveling Waves, Standing Waves, and the Dispersion Relation.* Phys 3750.

[13] I. A. Viktorov. (1967). *Rayleigh and Lamb Waves - Physical Theory and Applications.* Plenum Press. New York.

[14] G. Maidanik. (1981). *Extension and reformulation of Statistical Energy Analysis with use of Room Acoustics Concepts*, J. of Sound and Vibration, 78, p417.

[15] G. Maidanik, L. J. Maga. (1981). *Transition from a Non-reverberant to a Reverberant Dynamic System*, J. of Sound and Vibration, 78, p 397. [16] W. Kropp. (2003) *Technical Acoustics 1 - lecture 3.* Gothenburg: Chalmers University of Technology - Department of Applied Acoustics

[17] K. Graff. (1975). *Wave motion in elastic solids.* Oxford: Clarendon Press.

[18] J. W. S. Rayleigh. (1887). *On waves propagated along the plane surface of an elastic solid*. Proc. Lond. math. Soc. **17,** 4-11.

[19] D. Johansson, P. Comnell. (2010). *Statistical Energy Analysis - Development and implementation of an open source code in MATLAB/Octave*. G{oteborg: Chalmers University of Technology, Division of Applied Acoustics, Vibroacoustics Group.

[20] P. Svensson, M. Kleiner, R. Torres. (1998). *Audio Technology and Acoustics - Useful formulas.* Gothenburg, Sweden: Chalmers Unversity of Technology, Department of Applied Acoustics.

[21] A. C. Nilsson. (2000). *Vibroacoustics - Part 1.* Stockholm: KTH, Marcus Wallenberg Laboratory for Sound and Vibration Research.

[22] A. F. Ganghi (a). R. L. Wesson (b). (1978). *P-wave to Rayleigh wave Conversion Coefficients for Wedge Corners; Model Experiments.* (a) Department of Geophysics, Texas A&M University, College Station, Texas 77843. (b) Office of Earthquake Studies, U. S. Geological Survey, Reston, Virginia 22092.

[23] F. Jin (a). Z. Wang (a). K. Kishimoto (b). (2004). *Basic properties of Rayleigh surface wave propagation along curved surfaces*. (a) Department of Engineering Mechanics, Xi'an Jiatong University, Xi'an 710049, People's Republic of China. (b) Department of Mechanical and Control Engineering, Tokyo Institute of Technology, 2-12-1, O-okayama, Meguro-ku, Tokyo 152-8552, Japan.

[24] W. Kropp. (2003) *Technical Acoustics 1 - lecture 3*. Gothenburg: Chalmers University of Technology - Department of Applied Acoustics

[25] Elisolation HMT AB. (2014). *PA6G*. Laxå: Elisolation HMT AB

[26] M. J. Y. Clement. (1960). *The reflection and transmission of Rayleigh waves*. The University of British Columbia (August, 1961).

[27] S. Yu. Gurevich, Kh. B. Tolipov. (2003). *Diffraction of Surface Waves by the Edge of a Wedge*. South Ural State University, Chelyabinsk.

[28] I. A. Viktorov. (1966). *Physics of Application of Rayleigh and Lamb Ultrasonic Waves* [in Russian]. Nauka, Moscov.

[29] Kh. B. Tolipov. (1993). *Dynamic problem of the theory of elasticity for angular regions with homogeneous boundary conditions*. Prikl. Matem. Mekh. **57**, No. 5, 120-126.

[30]G. F. Miller, H. Pursey. (Dec. 6, 1955). *On the partition of energy between Elastic Waves in a half-infinite Solid*. Proceedings of the Royal Society of London. Series A, Mathematical and Physical Sciences, Vol. 233, No. 1192, pp. 44-69.

[31] C-W. Yu, M. Dravinski. (Feb. 19, 2009). *Scattering of plane harmonic P, SV or Rayleigh waves by a completely embedded corrugated cavity*. Department of Aerospace and Mechanical Engineering, University of Southern California, Los Angeles, CA 90089-1453.

[32] R. J. Blake*, L. J. Bond.+ (May 20, 1991). *Rayleigh wave scattering from surface features: up-steps and troughs.* * SERC Daresbury Laboratory, Keckwick Lane, Daresbury, Warrington WA4 4AD, Cheshire, UK. + National Institute of Standards and Technology, 325 Broadway, Boulder, Colorado 80303, USA and Department of Mechanical Engineering, University of Colorado at Boulder, Colorado 80309-0427, USA.

[33] R. J. Blake, L. J. Bond.* (Apr. 17, 1989). *Rayleigh wave scattering from surface features: wedges and down-steps.* * SERC Daresbury Laboratory, Keckwick Lane, Daresbury, Warrington, Cheshire WA4 4AD, UK Department of Mechanical Engineering, University College London, Torrington Place, London WC1 7JE, UK.

[34] S.V. Biryukov, Yu.V. Gulyaev, V.V. Krylov, V.P. Plessky. (1995) *Surface Acoustic Waves in Inhomogeneous medium.* Springer-Verlag, Berlin Heidelberg.

[35] J. Shinn. (2010). *Perturbation Theory and the WKB Method.* Department of Mathematics, Colorado State University, USA.

[36] Direct Industry. (2014). *jumbo-drilling-rigs-59040-3588385.jpg.* Retrieved 2014-08-28. Available: http://img.directindustry.com/images_di/photo-g/jumbo-drilling-rigs-59040-3588385.jpg.